LU TP 15-32

LUND UNIVERSITY
DEPARTMENT OF ASTRONOMY AND THEORETICAL PHYSICS

MASTER THESIS

Transverse Momentum Dependent Soft Function in SCET to NNLO

Author:
Joel Oredsson

Supervisor:
Johan Bijnens
Frank Tackmann

September 4, 2015

Abstract

We review the factorization theorem for the production of a heavy color-neutral final state with a transverse momentum much smaller than its invariant mass in the framework of soft collinear effective field theory (SCET). This phase space region is plagued by large logarithms of widely separated scales, including large logarithms of rapidity ratios, that need to be resummed for sensible results. In this thesis we use a recently developed formalism that introduces a rapidity regulator in addition to dimensional regularization. This results in an additional renormalization scale, which enables one to also resum rapidity logarithms. The factorized cross sections can be written as a product (convolution) of hard, beam and soft functions in position (momentum) space. We compute the soft function to next-to-next-to-leading-order (NNLO) and determine all relevant anomalous dimensions. Based on the known renormalization group structure, we perform an important cross check of the results by deriving an all order formula for the logarithmic structure of the soft and beam functions. This also allows us to obtain the beam functions to NNLO by comparing to known results in another scheme. With our results, one can now compute the transverse momentum distribution of Higgs production to next-to-next-to-leading-log-prime (NNLL$'$) accuracy. A new feature in this formalism is that one can directly perform the complete set of relevant scale variations in order to estimate the uncertainty in the resummed cross section.

Contents

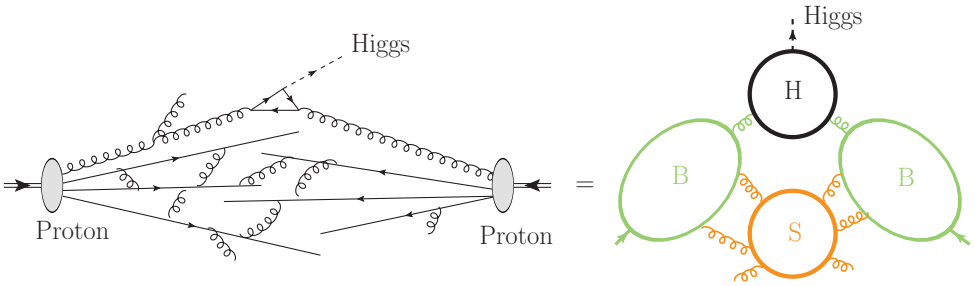

Figure 1: Med en effektiv teori kan man förenkla beräkningar av partikelkollisioner genom att faktorisera uträkningen till en hard-, två beam- och en soft-funktion.

Precisionsberäkningar för stark växelverkan

År 2012, efter många decenniers forskning, annonserades upptäckten av en Higgspartikel i Large Hadron Collider (LHC) vid Geneva. Första delen, av vad som kallas världens största experiment, var då klar och man kunde fastställa att man hade upptäckt en ny partikel med spin 0, en så kallad skalärpartikel. Denna partikel är oerhört betydelsefull då dess tillhörande fält är grundstenen Higgs-mekanism, en mekanism vars teoretiska ursprung belönades med nobelpriset 2013. Higgsfältet är grunden för att förena den svaga med den elektromagnetiska kraften och är ansvarig för att ge alla fundamentala partiklar dess massa. Detta är den sista pusselbiten i standardmodellen som beskriver de två nämnda krafterna plus den starka växelverkan.

Men även då standardmodellen stämmer överens med många experiment till oerhörd precision så finns det exempel på fenomen som den inte kan förklara. Ett exempel är mörk materia som det finns bevis för från astrofysiken men som hitintills inte har visat sig i några experiment utförda med acceleratorer. Det finns alltså nya upptäckter att göra vilket ytterligare betonar vikten av att studera Higgspartikeln för att finna ledtrådar till ny fysik.

LHC startade igen år 2015, efter en rad av uppgraderingar, med dubbla energin. Medan de experimentella fysikerna är upptagna med att ta fram bättre experimentella resultat så kommer teoretiska fysiker att uppfinna nya metoder att utföra precisionsberäkningar. Den största teoretiska utmaningen är att förstå den starka växelverkan vid partikelkollisioner. Det är nämligen väldigt komplicerat att göra analytiska beräkningar för hur kvarkar och gluoner interagerar med varandra, just därför att de interagerar med varandra så starkt. Detta är ett väsentligt problem i LHC då de där kolliderar protoner som består av kvarkar och gluoner. En bra förståelse för den starka växelverkan vid kollisioner är därför nödvändig för att kunna göra några slutsatser överhuvudtaget.

För att få kvantitativa resultat kan man använda Monte Carlo metoder och datorkraft för att simulera kollisioner. En annan väg är att förenkla teorin för det starka växelverkan med en effektiv teori. Genom att separera olika fysikaliska processer vid en partikelkollision kan man få fram en modell vilket möjliggör analytiska beräkningar.

I detta arbete har "Soft Collinear Effective Field Theory" använts, vilket är en nyutvecklad modell för att studera partikelkollisioner. Med hjälp av denna modell kan man beräkna olika processer som inneträffar i en kollision separat, vilket möjliggör förbättrad teoretisk precision jämfört med tidigare beräkningar.

Till exempel vid beräkningar av exakta sannolikheter för att producera en Higgspartikel vid LHC kan man säga att det finns tre distinkta faktorer. En så kallad hard-funktion som beskriver hur en kvark eller gluon skapar en Higgs. Innan de fusionerar till en Higgs så är de dock sammansatta till två separata protoner och man har två, i princip likadana, beam-funktioner som beskriver vardera kvark eller gluon. Till sist så behöver man inkludera hur dessa protoner interagerar med varandra genom svag strålning vilket sammanfattas med en soft-funktion.

Detta arbete kretsar runt denna sistnämnda faktor i en kollisionsprocess, en soft-funktion. För att beräkna den så använder man störningsräkning, vilket i kvantfältteori innebär att man kan uttrycka soft-funktionen som en summa av processer med minskande sannolikhet för att inträffa. Till en första approximation tar man endast med det största bidraget där man inte har någon soft strålning alls. Genom att ta med mer strålning i beräkningen så vinner man teoretisk precision och minskad osäkerhet i resultatet. Huvudmålet med detta arbete är att beräkna de första tre termerna av soft-funktionen.

Abbreviations

C-Web
Connected Web

EFT
Effective Field Theory

IR
InfraRed

LHC
Large Hadron Collider

PDF
Parton Distribution Function

QCD
Quantum ChromoDynamics

QED
Quantum ElectroDynamics

QFT
Quantum Field Theory

RRGE
Rapidity Renormalization Group Equation

RGE
Renormalization Group Equation

SCET
Soft Collinear Effective Field Theory

SM
Standard Model

TMDPDF
Transverse Momentum Dependent Parton Distribution Function

UV
UltraViolet

Chapter 1

Introduction

The discovery of a Higgs boson in 2012 at the Large Hadron Collider (LHC) [1][2] marked the beginning of a new paradigm in high energy physics. Never before has a fundamental scalar been observed in nature and this is a remarkable achievement, both experimentally and theoretically. Two of the physicists behind the mechanism that generates the masses of the W and Z gauge bosons were awarded the nobel prize in physics 2013 [3][4]. However, what kind of Higgs that has been found is now up for debate and precision measurements of its properties is necessary to discover its origin. So far the Higgs resembles the Standard Model (SM) Higgs, but questions remain about the exact structure of the Higgs sector. Even though the SM describes the electromagnetic, weak and strong force and agrees with collider experiments to an incredible accuracy, it cannot be the complete picture. New physics is needed to explain the big open questions in physics today; Such as the nature of dark matter and incorporation of gravity in a quantum theory.

Now in 2015, the LHC has started again after its first upgrade. To get hints of any new physics, physicists will continue to study collisions of protons at the LHC to probe nature at unprecedented energies. In any collision process at the LHC, precise theoretical predictions are important for comparing theory to the experimental data. One observable that is being measured is the differential cross section for the production of a Higgs boson as a function of its transverse momentum, $\mathbf{p}_\perp$. Such a study can be used to acquire a good understanding of the underlying production mechanism; as well as to search for new physics. To identify the Higgs' decays, the collision events are organized according to their highest-momentum jet and the bin with zero central jets over a certain threshold plays an essential role in the analysis since the region of small $\mathbf{p}_\perp$ dominates the number of events.

To make a theoretical prediction for this observable, or any other observable at the LHC, one requires precision calculations of processes in Quantum Chromodynamics (QCD). Since protons are made up out of strongly interacting particles, a good understanding of QCD processes is of utmost importance since QCD physics dominate at a proton collider. The fact that QCD is a strongly interacting theory however poses theoretical challenges. At large energies one can use perturbation theory to compute observables but in a collision process there are several separate energy scales that enter the calculations. These enter through large logarithms, of ratios of energy scales, that spoil the convergence of perturbation theory and in order to get a quantitative prediction one needs to account for all the largest terms in a perturbative expansion. This is referred to as resummation. The $\mathbf{p}_\perp$ spectrum of Higgs production is plagued by such large logarithms when $\mathbf{p}_\perp$ is much smaller than the Higgs mass and this thesis revolves

around making better precision calculations for such an observable with the help of an effective field theory.

Resummation and Effective Field Theories

To describe physics at the LHC, physicists have been doing lots of precision calculations in the SM. However it is sometimes very cumbersome to compute observables directly in the full theory. With good physical arguments one can separate the important degrees of freedom to get an Effective Field Theory (EFT), which makes calculations easier while still describing the same physics. It is not only an advantage in clearly separating the physics in a process, but EFTs can sometimes be crucial when the calculations in the full theory are too hard. One problem with different degrees of freedom that are associated with different energy scales is that perturbation theory can breakdown because of large logarithms. As an example, we write the $\mathbf{p}_\perp^2$ cross section for Higgs boson production schematically as

$$\begin{aligned}\frac{d\sigma}{d\mathbf{p}_\perp^2} \sim 1 + \alpha_s L^2 + \alpha_s^2 L^3 + \alpha_s^3 L^4 + \dots \text{ (LL)} \\ + \alpha_s L \ + \alpha_s^2 L^2 + \alpha_s^3 L^3 + \dots \text{ (NLL)} \\ + \alpha_s^2 L \ + \alpha_s^3 L^2 + \dots \text{ (NNLL)}.\end{aligned}$$

Now, if L is a logarithm of the hard scale, m_h, over momentum like $L = \log(m_h^2/\mathbf{p}_\perp^2)$ that is $\mathcal{O}\left(\alpha_s^{-1}\right)$, then all the terms in the first row, except the first unity term, are $\mathcal{O}\left(\alpha_s^{-1}\right)$ and all terms in the second row are $\mathcal{O}(1)$. To get a sensible result, both the first and second row need to be included in the result. Summing up the first row would corresponds to resummation of leading-logarithmic (LL) terms. To include the next row would be next-to-leading-logarithmic (NLL) resummation and so on.

One way of doing this resummation is to split up the logarithms into parts by introducing a renormalization scale that then acts as a cut off for the effective theory. An operator product expansion of the full theory matrix element does this by putting all the high energy physics in Wilson coefficients while keeping the low energy dynamical degrees of freedom in the EFT matrix elements. This can be sketched up for some observable O in the case of a single logarithm as

$$\begin{aligned}\langle O \rangle_{\text{full}} &\sim 1 + \alpha_s \log \frac{m_h^2}{\mathbf{p}_\perp^2} + \dots \\ &\sim \left(1 + \alpha_s \log \frac{m_h^2}{\mu^2} + \dots\right)\left(1 + \alpha_s \log \frac{\mu^2}{\mathbf{p}_\perp^2} + \dots\right) \equiv C(\mu)\,\langle O(\mu) \rangle_{\text{eff}}\,. \quad (1.1)\end{aligned}$$

The full theory clearly does not depend on the renormalization scale μ which leads to Renormalization Group Equations (RGE) for the Wilson coefficients. All the problems with the large logarithms can then be avoided if one matches the effective theory at the high scale m_h and then runs the Wilson coefficients down to $\mu^2 \sim \mathbf{p}_\perp^2$ with the RGE. This will effectively sum up all the large logarithms.

Soft Collinear Effective Theory

Soft Collinear Effective Field Theory (SCET) is a specific framework that disentangles the collinear and soft degrees of freedom of QCD in a collision process. SCET originated

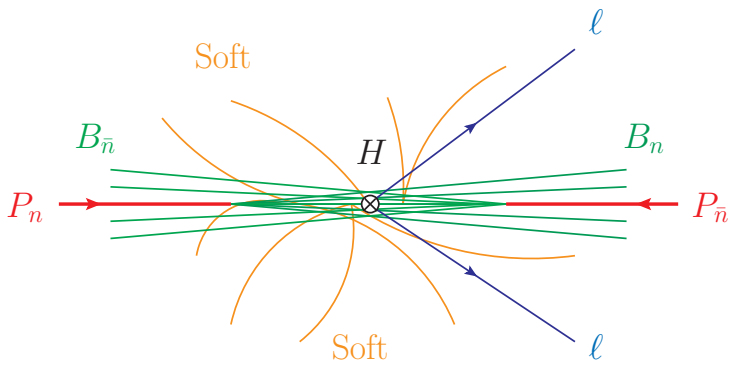

Figure 1.1: An example of an event shape for $pp \to XL$ with two leptons, ℓ, in the final state. The Beam functions, $B_{n,\bar{n}}$ describe the incoming partons as incoming jets while all the soft radiation is described by the Soft function, S. Hard fluctuations are integrated out and contribute to Wilson coefficients that are collected in the hard function, H.

from B physics where it can describe light decays of a B meson in its rest frame. Today, SCET features a range of applications such as the production of energetic jets in colliders and the scattering of energetic particles off a target at rest.

This thesis is centered around $pp \to XL$ processes at small transverse momentum, $\mathbf{p}_\perp$, of the color-singlet final state L, while X is the hadronic final state, see Fig. 1.1. As mentioned before, one example of such an observable that is of obvious importance is the Higgs production spectrum. The latest data from Run 1 of the LHC is displayed in Fig. 1.2. At large $\mathbf{p}_\perp^2$ this can be computed with fixed order perturbation theory, but the calculations are plagued by large logarithms in the low transverse momentum region $\mathbf{p}_\perp^2 \ll m_h^2$.

The large logarithms arise from the presence of multiple energy scales in the collision process. We will see how one can factorize the cross section into a hard function, H, responsible for the hard interaction; two beam functions, B, that describe an incoming jet along each collinear direction; and a soft function, S, which collects all soft radiation effects. For now, we write this schematically as

$$\frac{d\sigma}{d^2\mathbf{p}_\perp} \sim H(m_h, \mu) \times B(\mathbf{p}_\perp, \mu) \otimes_\perp B(\mathbf{p}_\perp, \mu) \otimes_\perp S(\mathbf{p}_\perp, \mu), \tag{1.2}$$

where the $\otimes_\perp$ denotes a convolution of the transverse momentum and μ is the ordinary renormalization scale from dimensional regularization.

The factorization due to SCET allows one to compute the three functions, H, B and S, separately in their respective perturbative regions. With the help of RGEs, all the factors in the cross section can then be evolved from their natural scale to a common arbitrary renormalization scale. This effectively resums all the large logarithms from every region. Since H describes the hard interaction at the high scale m_h, it will contain logarithms like $\log(m_h^2/\mu^2)$ and one can identify its natural scale which minimizes the logarithms to be $\mu_H^2 \sim m_h^2$. The beam functions describe the partons that participate in the collisions and they are matched onto ordinary parton distribution functions at some other, much smaller, scale $\mu_B^2 \sim \mathbf{p}_\perp^2$. All the soft interactions between the incoming partons as well as any soft radiation in the collision are contained in a soft function with its own natural soft scale $\mu_S^2 \sim \mathbf{p}_\perp^2$.

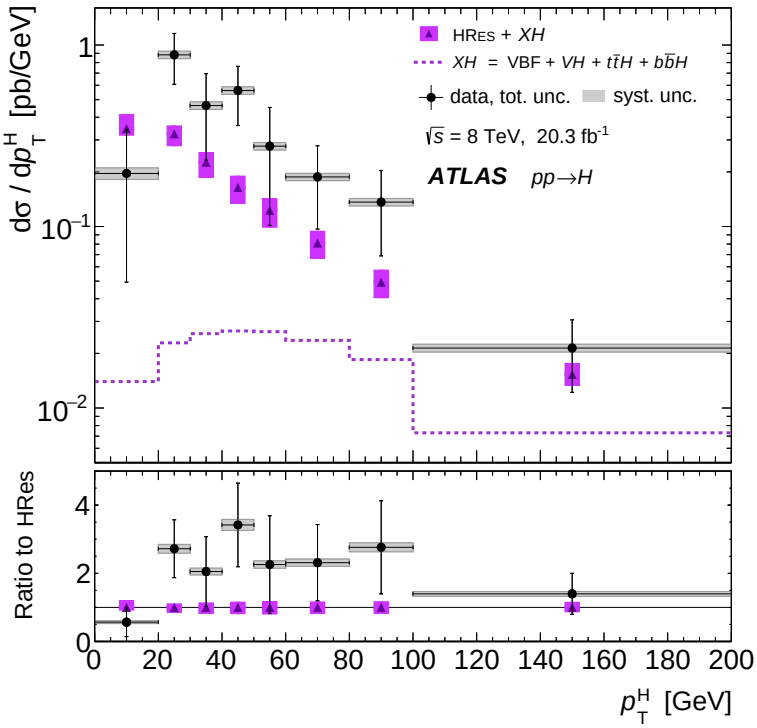

Figure 1.2: Differential cross section for Higgs boson production measured by the ATLAS collaboration. The data is from a combination of the $H \to \gamma\gamma$ and $H \to ZZ$ channels. Plot taken from [5].

Although a resummation framework has already been developed for this process a long time ago [6, 7], we will use the modern framework of SCET in Ref. [8, 9] to factorize the cross section. Using this framework, one encounters rapidity divergences in B and S that need to be regulated in addition to the ordinary UltraViolet (UV) and InfraRed (IR) divergences. The main objective of this thesis is to compute the soft function to NNLO and we will use the same analytic regulator as in Ref. [8, 9] in addition to dimensional regularization to handle all the divergences. This results in a rapidity renormalization scale ν, which is used much in the same way as the ordinary μ scale. The rapidity divergences are related to logarithms that will be resummed with Rapidity Renormalization Group Equations (RRGE). This has an advantage over previous resummation schemes because with two renormalization scales we can cleanly separate the running associated with different logarithms and thus probe the size of uncertainties from sub-leading logarithms more carefully.

The resummation of the Higgs $\mathbf{p}_\perp$ spectrum has previously been done in another SCET framework where the method of resumming rapidity logarithms is not based on a renormalization group [10]. The Beam functions have been computed to NNLO in this framework [12, 13] and we will translate their results to retrieve the beam functions to NNLO in our framework as well.

Outline

We will start off in Chap. 2 by describing the SCET framework that we will be working in and some of its features that are of importance in the following computation. In Chap. 3, we also go through the factorization theorem for $pp \to XL$ to see how the cross section factorizes into hard, soft and two beam functions.

The next two chapters are devoted to the computation of the soft function. The NLO is done in Chap. 4 while the technique to do the NNLO is described in Chap. 5.

All the parts of the soft function are combined and renormalized in Chap. 6 and, afterwards, we compute all the relevant anomalous dimensions. As a cross check of these results, we derive a recursive formula that determines the soft function's structure to all orders in Sec. 6.3. The $\mathcal{O}(\alpha_s^2)$ structure in position space can be found in Sec. 6.3.3.

After we have the final soft function results we use them to retrieve the beam functions in our framework to NNLO as well. We will translate the cross section, in the case of Higgs production, from another SCET framework, where the beam functions have been calculated to NNLO, to the framework which we use in this thesis in Chap. 7. Similar to the case of the soft function, we derive the full structure of the beam functions in Sec. 7.2; then match it onto the beam functions in the other scheme to retrieve the missing pieces and present the results in Sec. 7.3.

A set of appendices are collected with relevant details to the computations throughout the thesis. Constants and conventions regarding the renormalization procedure can be found in App. A; the Feynman rules for Wilson lines are derived in App. B; Hypergeometric functions and plus distributions, which will be used heavily in this thesis, are presented in appendices C and D, respectively; and finally the hard function in Higgs production through gluon fusion is written down in App. E.

Chapter 2

Soft Collinear Effective Theory

There are multiple energy scales that are of importance in a collision process. To probe physics at a hard scale Q we must disentangle it from other QCD physics that happens at lower scales, such as $\Lambda_{\rm QCD}$ or $p_\perp$. SCET is the appropriate framework to factorize the cross sections into distinct hard, collinear and soft factors by effectively separating the collinear and soft degrees of freedom of quarks and gluons [14, 15, 16, 17].

In this thesis we will consider $pp \to XL$ processes, where L represents any non-strongly interacting set of particles, while X is any hadronic final state, e.g. jets along the beam axis. Possible scenarios are Drell-Yan-like processes or Higgs production at the LHC. We will consider the phase-space region where the total transverse momentum, $\mathbf{p}_\perp^2$, of L is much smaller than the hard interaction scale, $Q^2 \sim m_h^2$ in the case of Higgs production. Then there are three relevant scales involved in the collision

$$\Lambda_{\rm QCD}^2 \ll \mathbf{p}_\perp^2 \ll Q^2$$

and our effective theory will be constructed such that $\lambda = |\mathbf{p}_\perp|/Q$ is a small expansion parameter. A good description of how the factorization works in $\rm SCET_I$ can be found in Ref. [18]. We will however be concerned with factorization in $\rm SCET_{II}$ and the difference between the two frameworks will be described below.

This chapter does not give a detailed review of the field-theoretic foundation and construction of SCET, but instead describes the smallest building blocks we need to match SCET currents onto QCD and factorize the cross section. The starting point is however to introduce light-cone coordinates which are the natural basis to describe collinear particles.

2.1 Light-Cone Coordinates

Collinear particles are characterized by having large energy and small invariant mass. When working with collinear particles it is very convenient to use light-cone coordinates. These are defined by two lightlike vectors, one $n^\mu = (1, \mathbf{n})$ to point along one beam direction and another $\bar{n}^\mu$ that satisfies

$$n^2 = \bar{n}^2 = 0, \qquad\qquad n \cdot \bar{n} = 2. \tag{2.1}$$

We use the bold notation to denote a vector in euclidean space. Although $\bar{n}^\mu$ is an arbitrary auxiliary vector, more often than not it is chosen to point in the opposite beam

direction. Any four-vector can then be decomposed in this basis by first defining

$$p^+ \equiv n \cdot p, \qquad\qquad p^- \equiv \bar{n} \cdot p.$$

Then we have

$$p^\mu = p^+ \frac{\bar{n}^\mu}{2} + p^- \frac{n^\mu}{2} + p_\perp^\mu \equiv (p^+, p^-, \mathbf{p}_\perp). \tag{2.2}$$

In the standard metric choice $(+ - --)$, the vector product will take the form

$$p \cdot k = \frac{1}{2}(p^+ k^- + p^- k^+) - \mathbf{p}_\perp \cdot \mathbf{k}_\perp, \qquad\qquad p^2 = p^+ p^- - \mathbf{p}_\perp^2. \tag{2.3}$$

Four-momenta	Invariant mass	Mode
$p_n^\mu \sim Q(\lambda^2, 1, \lambda)$	$p^2 \sim Q^2\lambda^2$	n-collinear
$p_{\bar{n}}^\mu \sim Q(1, \lambda^2, \lambda)$	$p^2 \sim Q^2\lambda^2$	$\bar{n}$-collinear
$p_s^\mu \sim Q(\lambda, \lambda, \lambda)$	$p^2 \sim Q^2\lambda^2$	soft
$p_{us}^\mu \sim Q(\lambda^2, \lambda^2, \lambda^2)$	$p^2 \sim Q^2\lambda^4$	ultra-soft
$p_G^\mu \sim Q(\lambda^2, \lambda^2, \lambda)$	$p^2 \sim Q^2\lambda^2$	Glauber

Table 2.1: Potential momenta scaling modes in light-cone coordinates.

An advantage of using light-cone coordinates is that the scaling of momenta appears very clearly as can be seen in Tab. 2.1. We can now analyze the different physical momenta for a final state L with small transverse momentum in terms of $\lambda = |\mathbf{p}_\perp|/Q$. The final state of a process, for example a Higgs boson, will have a momentum that scales as $p^\mu \sim Q(1, 1, \lambda)$ and radiation that recoils against this state will then have to have similar $p_\perp$ scaling; thus the collinear and soft are the relevant momentum modes for the approximately massless particles in X. The EFT for these degrees of freedom goes by the name SCET_II. In contrast, SCET_I includes the ultra-soft instead of the soft modes.

Even though it seems like the Glauber modes should be included in the EFT, it has been shown that they do not contribute to the process which we are concerned with[19].

2.2 SCET Ingredients

Particles in different collinear directions can exchange large momenta, Q, in a collision via off-shell modes. These hard fluctuations are integrated out and contribute to Wilson coefficients in the EFT Lagrangian. This is done by matching QCD onto SCET, which yields the hard function. In the next chapter on factorization, we will see how the degrees of freedom below the energy scale Q are divided into distinct collinear sectors. These only interact with each other through soft radiation, which factors out as well to yield the soft function.

Before going through the factorization of the cross section we will review the necessary ingredients of SCET. This discussion will be done in the framework of SCET_I which later on will be matched onto SCET_II. For a detailed explanation of all these building blocks we refer to the introduction notes in Ref. [20, 21] and the original literature [14, 15, 16, 17]. These building blocks of SCET are constructed from the full theory QCD by separating the ordinary fields into collinear and soft fields that carry specific momenta and expanding

systematically in some power counting parameter λ. Since the momentum components of the fields scale differently, it is convenient to split them up into two parts, the large label and small residual momenta.

The collinear fields in SCET are the quark and gluon fields, $\xi_{n,\tilde{p}}(x)$ and $A_{n,\tilde{p}}(x)$. They are labeled by their collinear direction n and large momentum $\tilde{p}$. By large momentum we here mean the collinear and transverse components, i.e. we split up the momentum as

$$p^\mu = \tilde{p}^\mu + k^\mu = \omega_n \frac{n^\mu}{2} + p_\perp^\mu + k^\mu. \tag{2.4}$$

The fields are then written in momentum space with respect to the large momentum while the dependence on residual momentum, k^μ, is expressed in position space. This allows us to define different derivative operations that have a definite scaling. So derivatives acting on the field pick out the residual momentum, $i\partial^\mu \sim k^\mu \sim \lambda^2$, while the large momentum is obtained by acting with a momentum operator on the field, $\mathcal{P}_n^\mu \sim \tilde{p}_n^\mu \sim (0, 1, \lambda)$. We also define the shorthand notation $\bar{\mathcal{P}}_n \equiv \bar{n} \cdot \mathcal{P}_n$.

To construct the leading order Lagrangian for SCET one splits up all the full theory QCD fields, identify their scaling in λ and expand. This analysis finds that the collinear quark fields scale as $\xi_n \sim \lambda$ while the gluons scale as their momentum, i.e. $A_n^\mu \sim (\lambda^2, 1, \lambda)$ and $A_s^\mu \sim (\lambda, \lambda, \lambda)$. The fact that $\bar{n} \cdot A_n \sim \mathcal{O}(1)$ means that one can include an infinite number of n-collinear gluons accompanying the n-collinear quarks at the same order in the power counting of λ. The emission of an infinite number of n-collinear gluons generated in the interaction of a n-collinear quark with a $\bar{n}$-collinear quark organizes into a Wilson line, which has the definition

$$W_n(x) = \left[\sum_{\text{perms}} \exp\left(\frac{-g}{\bar{\mathcal{P}}_n} \bar{n} \cdot A_n(x) \right) \right]. \tag{2.5}$$

We also define a collinear covariant derivative

$$iD_{n_\perp}^\mu = \mathcal{P}_{n_\perp}^\mu + gA_{n_\perp}^\mu, \tag{2.6}$$

and write collinearly gauge invariant quark and gluon fields as

$$\chi_{n,\omega}(x) = \left[\delta(\omega - \bar{\mathcal{P}}_n) W_n^\dagger(x) \xi_n(x) \right], \tag{2.7}$$

$$\mathcal{B}_{n,\omega}^\mu(x) = \frac{1}{g} \left[\delta(\omega + \bar{\mathcal{P}}_n) W_n^\dagger(x) iD_{n_\perp}^\mu W_n(x) \right]. \tag{2.8}$$

Here, the momentum operator acts on every field to its right. The label momentum ω is a continuous parameter equal to the sum over all the minus momentum inside the brackets, while the large label momenta, $\tilde{p}$, of the individual fields are summed over,

$$\xi_n(x) = \sum_{\tilde{p}} e^{-i\tilde{p}\cdot x} \xi_{n,\tilde{p}}(x), \tag{2.9}$$

which we suppress in our notation.

The leading-order SCET_I Lagrangian for collinear quarks reads

$$\mathcal{L}_n = \bar{\xi}_n \left(in \cdot D_{us} + gn \cdot A_n + i\not{D}_{n_\perp} W_n \frac{1}{\bar{\mathcal{P}}_n} W_n^\dagger i\not{D}_{n_\perp} \right) \frac{\not{\bar{n}}}{2} \xi_n, \tag{2.10}$$

where the quarks couple ultra-soft gluons through the ultra-soft covariant derivative

$$iD^{\mu}_{us} = i\partial^{\mu} + gA^{\mu}_{us}. \tag{2.11}$$

The coupling of soft gluons and collinear particles can be removed at leading order with the field redefinitions

$$\begin{aligned} \chi^{(0)}_{n,\omega}(x) &= Y^{\dagger}_{n}(x)\chi_{n,\omega}(x), \\ \mathcal{B}^{\mu(0)}_{n,\omega_{\perp}}(x) &= Y^{\dagger}_{n}(x)\mathcal{B}^{\mu}_{n,\omega_{\perp}}(x)Y_{n}(x), \end{aligned} \tag{2.12}$$

where $Y_n(x)$ is a ultra-soft Wilson line in the fundamental representation

$$Y_n(x) = \mathbf{P}\exp\left[ig\int_{-\infty}^{0} dsn\cdot A_{us}(x+sn)\right]. \tag{2.13}$$

The $\mathrm{SCET_I}$ Lagrangian then separates as

$$\mathcal{L}_{\mathrm{SCET}} = \sum_i \mathcal{L}_{n_i} + \mathcal{L}_{us} + (\ldots), \tag{2.14}$$

where the $(\ldots)$ denotes subleading terms in λ. The leading order terms in the Lagrangian is decomposed into distinct sectors $\mathcal{L}_{n_i}$ and $\mathcal{L}_{us}$ that do not interact anymore. This a key point that allows us to factorize the cross section into collinear and soft functions. The consequence of the field redefinitions is that ultra-soft interaction between different collinear directions decouple by introducing ultra-soft Wilson lines in the external currents. In the cross section, these ultra-soft Wilson lines can be factored out of the matrix elements to create a separate soft function which then will be a vacuum matrix element of Wilson lines. The soft function is the focus of this thesis and we will calculate it to NNLO in the following chapters.

Chapter 3

Factorization

3.1 Cross Section in QCD

As previously stated we will consider the cross section for $pp \to XL$, where L can be any non-strongly interacting particles, while X stands for the hadronic final state, see Fig. 1.1. This could be a Drell-Yan process or Higgs production through gluon fusion where the Higgs then decays non-hadronically. A proper derivation of the factorization theorem in SCET_I can be found in Ref. [18] and we will here follow their formalism, however with a SCET_II measurement.

For any process where the hard partonic interaction is through a single two-parton QCD current, we can write the full-theory matrix element as

$$\mathcal{M}(pp \to XL) = \sum_J J_L \langle X| J |pp\rangle , \tag{3.1}$$

where the sum runs over all color-singlet two-particle QCD currents J. The J_L is the color-singlet part of the matrix element that we will not pay any closer attention to in this thesis.

The cross section for $\mathbf{p}_\perp$ measurement in full QCD can now be factorized into a leptonic and a hadronic part like

$$\begin{aligned}\frac{d\sigma}{d\mathbf{p}_\perp^2} = \frac{1}{2E_{\text{cm}}^2}\int\frac{d^4q}{(2\pi)^4}\int d\Phi_L (2\pi)^4\delta^{(4)}(q-p_L)\frac{1}{4}\sum_{\text{spins}}\sum\!\!\!\!\!\!\int_X |\mathcal{M}(pp\to XL)|^2 \\ \times\,\delta(\mathbf{p}_\perp^2 - \mathbf{p}_{X_\perp}^2)(2\pi)^4\delta^{(4)}(P_a+P_b-q-p_X) \\ \equiv \frac{1}{8E_{\text{cm}}^2}\sum_{J,J'}\int\frac{d^4q}{(2\pi)^4}L_{J,J'}(q)W_{J,J'}(q,\mathbf{p}_\perp).\end{aligned} \tag{3.2}$$

The integration of $d\Phi_L$ is over L's phase space and the hadronic phase space integration is contained in $\sum\!\!\!\!\!\!\int_X$. P_a and P_b are the incoming proton momenta while p_X and p_L are the total hadronic and color-singlet momenta, respectively. We have defined the color-singlet factor

$$L_{J,J'}(q) = \int d\Phi_L (2\pi)^4\delta^{(4)}(q-p_L) J_L^\dagger J_L', \tag{3.3}$$

and the hadronic matrix element

$$W_{J,J'}(q,\mathbf{p}_\perp) = \sum\!\!\!\!\!\!\int_X \langle pp|\, J^\dagger(0)\,|X\rangle\,\langle X|\,J'(0)\,|pp\rangle\,(2\pi)^4\delta^{(4)}(P_a+P_b-q-p_X)\delta(\mathbf{p}_\perp^2-\mathbf{p}_{X_\perp}^2)$$
$$= \int d^4x e^{-iq\cdot x}\,\langle pp|\,J^\dagger(x)\delta(\mathbf{p}_\perp^2-\mathcal{P}_\perp^2)J'(0)\,|pp\rangle\,, \quad (3.4)$$

where the 2-dimensional delta function picks out the measurement of transverse momentum.

3.2 Matching onto SCET

The full QCD current can be matched onto two SCET operators, one for each collinear direction, which means we integrate out the hard fluctuations. To go to $\mathrm{SCET_{II}}$, we will formally match $\mathrm{SCET_I}$ onto $\mathrm{SCET_{II}}$. This can be pictured as lowering the virtuality of the collinear sectors to the same invariant mass scale as the soft modes. Effectively, this works such that the factorization is done in the same way for $\mathrm{SCET_{II}}$ as for $\mathrm{SCET_I}$, with the substitution of soft Wilson lines, instead of ultra-soft, in the operators [17, 22], i.e. we make the substitution

$$Y_n^i(x) \to S_n^i(x) = \mathbf{P}\exp\left[ig\int_{-\infty}^0 dsn\cdot A_s(x+sn)\right] \quad (3.5)$$

in the SCET operators. Here, $i=q$ for a Wilson line in the fundamental representation and $i=g$ in the adjoint representation.

We will write the SCET current, with operators in momentum space with respect to the large momenta, as

$$J(x) = \sum_{n_1,n_2}\int d\omega_1 d^2\mathbf{p}_{1_\perp}\int d\omega_2 d^2\mathbf{p}_{2_\perp}\int d^4p_s e^{-i(p_1+p_2+p_s)\cdot x}$$
$$\times\left[\sum_q C_{q\bar q}^{\alpha\beta}(\omega_1,\omega_2)O_{q\bar q}^{\alpha\beta}(p_1,p_2,p_s,x) + C_{gg}^{\mu\nu}(\omega_1,\omega_2)O_{gg_{\mu\nu}}(p_1,p_2,p_s,x)\right]. \quad (3.6)$$

Here $p_i^\mu = \omega_1\frac{n_i^\mu}{2} + p_{i_\perp}^\mu$, where ω_i denotes the $\mathcal{O}(1)$ momentum while $p_{i_\perp}^\mu$ is the $\mathcal{O}(\lambda)$ momentum and p_s is the soft momentum of the Wilson lines. All the x dependence now corresponds to purely residual momenta.

The leading order operators in SCET after the field redefinitions in Eq. (2.12) are

$$O_{q\bar q}^{\alpha\beta}(p_1,p_2,p_s,x) = \bar\chi_{n_1,-p_1}^{(0)\alpha j}(x)T\left[{S_{n_1}^q}^\dagger(x)S_{n_2}^q(x)\right]_{-p_s}^{jk}\chi_{n_2,p_2}^{(0)\beta k}, \quad (3.7)$$
$$O_{gg}^{\mu\nu}(p_1,p_2,p_s,x) = \sqrt{\omega_1\omega_2}\mathcal{B}_{n_1,-p_1,\perp}^{(0)\mu c}(x)T\left[{S_{n_1}^q}^\dagger(x)S_{n_2}^q(x)\right]_{-p_s}^{cd}\mathcal{B}_{n_2,-p_2,\perp}^{(0)\nu d}. \quad (3.8)$$

Where j and c are color indices and α,β are spinor indices. The S^q and S^g are Wilson lines in the fundamental and adjoint representation, respectively, and the time ordering is required to ensure the proper ordering of the soft gluon fields in the Wilson lines. The fields are defined as

$$\chi_{n_i,p_i}^{(0)j}(x) = \delta(\omega_i-\mathcal{P}_{n_i})\delta^{(2)}(\mathbf{p}_{i_\perp}-\mathcal{P}_{n_{i\perp}})\chi_{n_i}^{(0)j}(x), \quad (3.9)$$
$$\mathcal{B}_{n_i,-p_i,\perp}^{(0)\mu a}(x) = \delta(\omega_i-\mathcal{P}_{n_i})\delta^{(2)}(\mathbf{p}_{i_\perp}-\mathcal{P}_{n_{i\perp}})\mathcal{B}_{n_i,\perp}^{(0)\mu a}(x), \quad (3.10)$$
$$T\left[{S_{n_1}^i}^\dagger(x)S_{n_2}^i(x)\right]_{-p_s}^{cd} = \delta^{(4)}(p_s-\mathcal{P})T\left[{S_{n_1}^i}^\dagger(x)S_{n_2}^i(x)\right]^{cd}, \quad (3.11)$$

where $i = \{q, g\}$. From here on we will suppress the (0) notation. If we just focus on the quark operator with an implicit sum over quark flavors, we get after plugging Eq. (3.6) into the hadronic matrix element

$$W(q, \mathbf{p}_\perp) = \sum_{n_1, n_2, n_1', n_2'} C_{q\bar{q}}^{\dagger\beta\alpha} C_{q\bar{q}}^{\alpha'\beta'} \left(\prod_i \int d\omega_i d^2\mathbf{p}_i \right) \int d^4p_s \int d^4x e^{-iq\cdot x} e^{i(p_1+p_2+p_s)\cdot x} \times \langle pp | \, O_{q\bar{q}\beta\alpha}^\dagger \delta(\mathbf{p}_\perp^2 - \mathcal{P}_\perp^2) O_{q\bar{q}\alpha'\beta'} \, | pp \rangle \, . \quad (3.12)$$

Now we can use the crucial fact that the different sectors of collinear and soft degrees of freedom separate at the Lagrangian level, which allows us to split the matrix element up into three parts with

$$|pp\rangle = |p_n\rangle \, |p_{\bar{n}}\rangle \, |0\rangle \, . \quad (3.13)$$

The measurement function can then also be split up like

$$\delta(\mathbf{p}_\perp^2 - \mathcal{P}_\perp^2) = \int d^2\boldsymbol{\ell}_{n_\perp} d^2\boldsymbol{\ell}_{\bar{n}_\perp} d^2\boldsymbol{\ell}_{s_\perp} \delta(\mathbf{p}_\perp^2 - |\boldsymbol{\ell}_{n_\perp} + \boldsymbol{\ell}_{\bar{n}_\perp} + \boldsymbol{\ell}_{s_\perp}|^2) \times \delta^{(2)}(\boldsymbol{\ell}_{n_\perp} - \mathcal{P}_{n_\perp}) \delta^{(2)}(\boldsymbol{\ell}_{\bar{n}_\perp} - \mathcal{P}_{\bar{n}_\perp}) \delta^{(2)}(\boldsymbol{\ell}_{s_\perp} - \mathcal{P}_{s_\perp}), \quad (3.14)$$

where each momentum operator $\mathcal{P}_{i_\perp}$ only picks out the momentum in its respective sector.

We are now ready to factorize the matrix element in Eq. (3.12) into two collinear and one soft matrix elements. The sums over collinear directions gives a factor of 4 and the result is

$$\begin{aligned}
W(q, \mathbf{p}_T) &= 4 C_{q\bar{q}}^{\dagger\beta\alpha} C_{q\bar{q}}^{\alpha'\beta'} \int d^2\boldsymbol{\ell}_{n_\perp} d^2\boldsymbol{\ell}_{\bar{n}_\perp} d^2\boldsymbol{\ell}_{s_\perp} \delta(\mathbf{p}_\perp^2 - |\boldsymbol{\ell}_{n_\perp} + \boldsymbol{\ell}_{\bar{n}_\perp} + \boldsymbol{\ell}_{s_\perp}|^2) \\
&\quad \times \int d\omega_n d^2\mathbf{p}_{n_\perp} d\omega_{\bar{n}} d^2\mathbf{p}_{\bar{n}_\perp} \int d^4p_s \int d^4x e^{-iq\cdot x} e^{i(p_n + p_{\bar{n}} + p_s)\cdot x} \\
&\quad \times \theta(\omega_n) \langle p_n | \, \bar{\chi}_n^{\beta k}(x) \delta(\omega_n - \bar{\mathcal{P}}_n) \delta^{(2)}(\mathbf{p}_{n_\perp} - \mathcal{P}_{n_\perp}) \delta^{(2)}(\boldsymbol{\ell}_{n_\perp} - \mathcal{P}_{n_\perp}) \chi_n^{\beta' k'}(0) \, | p_n \rangle \\
&\quad \times \theta(\omega_{\bar{n}}) \langle p_{\bar{n}} | \, \chi_{\bar{n}}^{\alpha j}(x) \delta(\omega_{\bar{n}} - \bar{\mathcal{P}}_{\bar{n}}) \delta^{(2)}(\mathbf{p}_{\bar{n}_\perp} - \mathcal{P}_{\bar{n}_\perp}) \delta^{(2)}(\boldsymbol{\ell}_{\bar{n}_\perp} - \mathcal{P}_{\bar{n}_\perp}) \bar{\chi}_{\bar{n}}^{\alpha' j'}(0) \, | p_{\bar{n}} \rangle \\
&\quad \times \langle 0 | \, \bar{T} \left[S_n^{q\dagger}(x) S_{\bar{n}}^q(x) \right]^{kj} \delta^{(4)}(p_s - \mathcal{P}_s) \delta^{(2)}(\boldsymbol{\ell}_s - \mathcal{P}_\perp) T \left[S_{\bar{n}}^{q\dagger}(0) S_n^q(0) \right]^{j'k'} | 0 \rangle \\
&= 4 C_{q\bar{q}}^{\dagger\beta\alpha} C_{q\bar{q}}^{\alpha'\beta'} \int d^2\mathbf{p}_{n_\perp} d^2\mathbf{p}_{\bar{n}_\perp} d^2\mathbf{p}_{s_\perp} \delta(\mathbf{p}_\perp^2 - |\mathbf{p}_{n_\perp} + \mathbf{p}_{\bar{n}_\perp} + \mathbf{p}_{s_\perp}|^2) \\
&\quad \times \int d\omega_n d\omega_{\bar{n}} \int d^4x e^{-iq\cdot x} e^{i(\omega_n x^+ + \omega_{\bar{n}} x^-)/2} e^{-i(\mathbf{p}_{n_\perp} + \mathbf{p}_{\bar{n}_\perp} + \mathbf{p}_{s_\perp})\cdot \mathbf{x}} \\
&\quad \times M_n(\omega_n, \mathbf{p}_n, x) M_{\bar{n}_\perp}(\omega_{\bar{n}}, \mathbf{p}_{\bar{n}_\perp}, x) M_s(\mathbf{p}_{s_\perp}, x). \quad (3.15)
\end{aligned}$$

In the last step we dropped the $p_s^\pm \sim \mathcal{O}(\lambda)$ momentum in the exponential. We have also defined the matrix elements

$$M_n(\omega_n, \mathbf{p}_{n_\perp}, x^-) = \theta(\omega_n) \langle p_n | \, \bar{\chi}_n^{\beta k}(x) \delta(\omega_n - \bar{\mathcal{P}}_n) \delta^{(2)}(\mathbf{p}_{n_\perp} - \mathcal{P}_{n_\perp}) \chi_n^{\beta' k'}(0) \, | p_n \rangle \, , \quad (3.16)$$

$$M_{\bar{n}}(\omega_{\bar{n}}, \mathbf{p}_{\bar{n}_\perp}, x^+) = \theta(\omega_{\bar{n}}) \langle p_{\bar{n}} | \, \chi_{\bar{n}}^{\alpha j}(x) \delta(\omega_{\bar{n}} - \bar{\mathcal{P}}_{\bar{n}}) \delta^{(2)}(\mathbf{p}_{\bar{n}_\perp} - \mathcal{P}_{\bar{n}_\perp}) \bar{\chi}_{\bar{n}}^{\alpha' j'}(0) \, | p_{\bar{n}} \rangle \, , \quad (3.17)$$

$$M_s(\mathbf{p}_{s_\perp}) = \langle 0 | \, \bar{T} \left[S_n^{q\dagger}(0) S_{\bar{n}}^q(0) \right]^{kj} \delta^{(2)}(\mathbf{p}_s - \mathcal{P}_\perp) T \left[S_{\bar{n}}^{q\dagger}(0) S_n^q(0) \right]^{j'k'} | 0 \rangle \, . \quad (3.18)$$

The residual x dependence associated with the large momentum in each matrix element have has absorbed, thus the only x dependence left is the residual in each collinear sector.

This can however also be dropped by Fourier transforming the matrix elements and do the x integral in Eq. (3.15), giving

$$\begin{aligned}
&\int d^4x e^{-iq\cdot x} e^{i(\omega_n x^+ + \omega_{\bar n} x^-)/2} e^{-i(\mathbf{p}_{n_\perp}+\mathbf{p}_{\bar n_\perp}+\mathbf{p}_{s_\perp})\cdot \mathbf{x}} M_n(x^-) M_{\bar n}(x^+) \\
&\qquad = \int \frac{dk_n^+}{(2\pi)} \int \frac{dk_{\bar n}^-}{(2\pi)} \tilde M_n(k_n^+) \tilde M_{\bar n}(k_{\bar n}^-) \\
&\qquad \times 2(2\pi)^4 \delta(\omega_n - q^- - k_n^- - k_{\bar n}^-) \delta(\omega_{\bar n} - q^+ - k_n^+ - k_{\bar n}^+) \\
&\qquad \times \delta^{(2)}(\mathbf{p}_{n_\perp} + \mathbf{p}_{\bar n_\perp} + \mathbf{p}_{s_\perp} + \mathbf{q}_\perp) \\
&= M_n(0) M_{\bar n}(0) 2(2\pi)^4 \delta(\omega_n - q^-) \delta(\omega_{\bar n} - q^+) \delta^{(2)}(\mathbf{p}_{n_\perp} + \mathbf{p}_{\bar n_\perp} + \mathbf{p}_{s_\perp} + \mathbf{q}_\perp) + \mathcal{O}(\lambda)
\end{aligned} \tag{3.19}$$

The $k_i \sim \mathcal{O}(\lambda^2)$ momentum is the residual momentum and in the last step we expanded around the momenta and only kept the lowest order in the power expansion for each delta function. Afterwards, one can do the k_i integrals which gives the matrix elements evaluated at $x = 0$.

Now we can do the ω integrals to get

$$\int d\omega_n \delta(\omega_n - q^-) M_n(0) = \frac{\not n^{\beta\beta'} \delta^{kk'}}{4N_c} \theta(q^-) \langle p_n | \, \bar\chi_n(0) \delta(q^- - \bar{\mathcal{P}}) \delta^{(2)}(\mathbf{p}_{n_\perp} - \mathcal{P}_{n_\perp}) \frac{\bar{\not n}}{2} \chi_n(0) \, | p_n \rangle \tag{3.20}$$

and similarly for the $\bar n$ part. Finally, the hadronic factor takes the form

$$\begin{aligned}
W(q, \mathbf{p}_\perp) &= \frac{2(2\pi)^4}{\pi N_c} \mathrm{Tr}_{\mathrm{spins}} \left\{ \frac{\not n}{2} \bar C_{q\bar q} \frac{\bar{\not n}}{2} C_{q\bar q} \right\} \delta(\mathbf{p}_\perp^2 - \mathbf{q}_\perp^2) \\
&\times \int d^2\mathbf{p}_{n_\perp} d^2\mathbf{p}_{\bar n_\perp} d^2\mathbf{p}_{s_\perp} \delta(\mathbf{p}_\perp^2 - |\mathbf{p}_{n_\perp} + \mathbf{p}_{\bar n_\perp} + \mathbf{p}_{s_\perp}|^2) B_q(q^-, \mathbf{p}_{n_\perp}) B_{\bar q}(q^+, \mathbf{p}_{\bar n_\perp}) S^q(\mathbf{p}_{s_\perp}),
\end{aligned} \tag{3.21}$$

where we have defined the quark beam and soft functions,

$$B_q(q^-, \mathbf{p}_{n_\perp}) = \theta(q^-) \langle p_n | \, \bar\chi_n(0) \delta(q^- - \bar{\mathcal{P}}) \delta^{(2)}(\mathbf{p}_{n_\perp} - \mathcal{P}_{n_\perp}) \frac{\not n}{2} \chi_n(0) \, | p_n \rangle \,, \tag{3.22}$$

$$S^q(\mathbf{p}_{s_\perp}) = \frac{1}{N_c} \langle 0 | \, \mathrm{Tr} \left\{ \bar T \left[S_n^{q\dagger}(0) S_{\bar n}^q(0) \right] \delta^{(2)}(\mathbf{p}_s - \mathcal{P}_\perp) T \left[S_{\bar n}^{q\dagger}(0) S_n^q(0) \right] \right\} | 0 \rangle \,. \tag{3.23}$$

If we now combine everything we get a final expression for the cross section as

$$\begin{aligned}
\frac{d\sigma}{d\mathbf{p}_\perp^2} &= \int \frac{d^4q}{(2\pi)^4} H(q^+, q^-) L(q) \delta(\mathbf{p}_\perp^2 - \mathbf{q}_\perp^2) \\
&\times \int d^2\mathbf{p}_{n_\perp} d^2\mathbf{p}_{\bar n_\perp} d^2\mathbf{p}_{s_\perp} \delta(\mathbf{p}_\perp^2 - |\mathbf{p}_{n_\perp} + \mathbf{p}_{\bar n_\perp} + \mathbf{p}_{s_\perp}|^2) B_q(q^-, \mathbf{p}_{n_\perp}) B_{\bar q}(q^+, \mathbf{p}_{\bar n_\perp}) S^q(\mathbf{p}_{s_\perp}),
\end{aligned} \tag{3.24}$$

where we collected the prefactors in the hard function

$$H(q^-, q^+) = \frac{(2\pi)^3}{2E_{\mathrm{cm}}^2 N_c} \mathrm{Tr}_{\mathrm{spins}} \left\{ \frac{\not n}{2} \bar C_{q\bar q} \frac{\bar{\not n}}{2} C_{q\bar q} \right\}. \tag{3.25}$$

After matching QCD onto SCET, the general result is a factorized cross section where the beam functions are in two distinct collinear sectors that do not interact with each other.

All the soft interaction is moved into the soft function. Both the beam and soft functions are therefore process independent and only differ depending on whether we match onto quark or gluon currents and the observable. All the process dependence is in the hard function and the color singlet matrix element, which then can be modified to fit whatever process one is interested in.

3.3 Rapidity Divergences

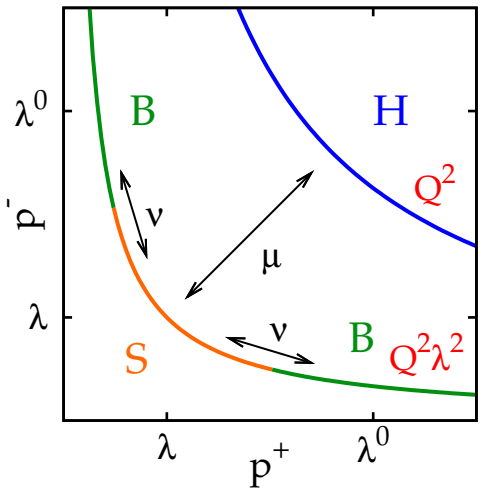

Figure 3.1: The beam (B) and soft (S) functions live on the same mass-shell hyperbola, $p^2 \sim Q^2\lambda^2$, while the hard (H) function lives at the high scale $p^2 \sim Q^2$. The arrows represent running of the functions in rapidity, ν, and virtuality scale, μ.

The beam and soft function in the cross section exhibit rapidity divergences, which arise from the factorization procedure. They are neither UV nor IR in nature and are absent in the full QCD theory. They have their origin in momentum regions where the invariant mass k^2 is held fixed while k^+/k^- or k^-/k^+ diverges. The rapidity divergences are related to logarithms from integrals such as

$$I = \int_\mu^Q \frac{dk^+}{k^+} = \log\frac{Q}{\mu}, \tag{3.26}$$

which range over both the soft and the collinear limit. Through the factorization process the EFT introduces a cut-off between the different regions with the scaling $Q \ll \Lambda \ll \mu$. In each respective sector one then takes the limits $\Lambda \to \infty/0$, which introduces divergences; consequently the divergent integral splits up like

$$I = \int_\mu^\Lambda \frac{dk^+}{k^+} + \int_\Lambda^Q \frac{dk^+}{k^+} \to \int_\mu^\infty \frac{dk^+}{k^+} + \int_0^Q \frac{dk^+}{k^+}. \tag{3.27}$$

From this picture, we see that every sector only depends on one scale and that this generates divergences that only cancel in the sum of the soft and collinear regions.

The rapidity divergences are a feature of SCET_II, where the soft and collinear sectors share the same invariant mass scaling. One can think of the rapidity divergences as

living on the boundary between the soft and collinear sectors[1]. The non-cancellation of the divergences within each separate sector changes the renormalization group structure of the theory and it is this fact that will allow us to perform the resummation of rapidity logarithms.

These divergences are not regulated with dimensional regularization and we will therefore use a second regulator that introduces an additional renormalization scale ν. The fact that the full theory is free of any rapidity divergences, and hence independent on ν, makes it possible to derive a Rapidity Renormalization Group Equation (RRGE)[9, 8]. Resummation of rapidity logarithms is then done by evolving the beam and soft function in rapidity scale. The degrees of freedom and RGE running of SCET_{II} are illustrated in Fig. 3.1.

3.3.1 Rapidity regulator

To compute the soft function in the following chapters, we need to regulate the rapidity divergences. As mentioned before, dimensional regularization is not enough and we will here use an additional rapidity regulator that was introduced in Ref. [9, 8]. The implementation of it effectively works as follows: for every Connected Web(C-Web) in a soft eikonal diagram, we introduce a factor

$$w^2 \left(\frac{\nu}{|2\mathcal{P}_{g3}|} \right)^{\eta} \tag{3.28}$$

in the integrals over loop momenta. In analogy to the μ scale in dimensional regularization, this introduces the dimensionful parameter ν that serves as a rapidity cut-off. The momentum operator $|2\mathcal{P}_{g3}|$ picks out the group momentum component $k^3 = \frac{1}{2}(k^+ - k^-)$ flowing through the C-Web. Similar to ϵ in dimensional regularization, the soft function will be expanded around $\eta = 0$ in the renormalization process.

To make out what exactly a C-Web is, we first state a well known fact of the soft function: it can be written in an exponential form in position space, see Sec. 5.3. Just as the contributions to the soft function can be represented by diagrams, the contributions to the exponent of the soft function can be represented by C-Webs. A useful fact about the C-Webs is that each one contains a color factor that is not present in a C-Web of lower order in α_s; hence they can be organized by their distinct color structure. This means that one can calculate the C_F^2 part of the soft function from the NLO part, since it is proportional to C_F. This is called the non-abelian exponentiation theorem[23, 24] and we will in this thesis assume that this regulator preserves it as argued in Ref. [8]. We will use this exponentiation theorem in Sec. 5.3 to obtain the 2-loop C_F^2 piece. However it would be interesting to show that the regulator indeed preserves exponentiation by explicit calculations of the C_F^2 diagrams. The computations of some of the C_F^2 diagrams are however a little bit more complicated since they are composed out of two C-Webs and thus require two factors of Eq. (3.28) in the integration. These sort of calculations are somewhat beyond the scope of this thesis and are left to future work.

With this regulator, the soft function will exhibit $1/\eta^n$ divergences as well as the usual dimensional regularization $1/\epsilon^n$ terms. When expanding the result, it is very important to expand in η before expanding in ϵ; more details can be found in Sec. 4.2 below.

[1] These kinds of integrals do not pose a problem in SCET_{I}, where the divergences cancel within each collinear and ultra-soft sector in the sum of all graphs including zero-bin subtractions.

We also introduced w as a "book-keeping" parameter which will play a role when deriving the ν anomalous dimension. It is analogous to a bare coupling constant which is made dimensionless by introducing a dimensionful parameter ν, just as ordinary couplings in the $\overline{\text{MS}}$ scheme. Requiring that the product $w^2\nu^\eta$ is ν independent leads to a "renormalization" of w, making it obey the RGE equation

$$\nu\frac{d}{d\nu}w = -\frac{\eta}{2}w. \tag{3.29}$$

Chapter 4

Soft function at NLO

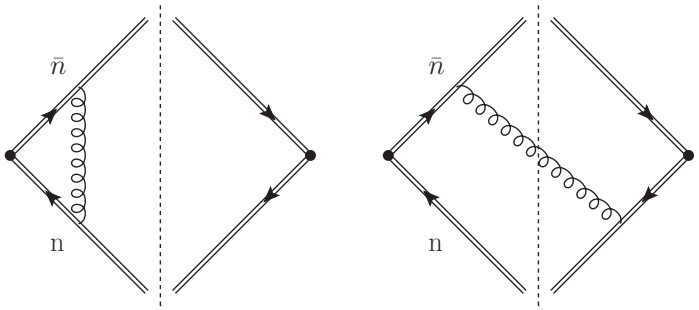

(a) (b)

Figure 4.1: NLO contributions to the soft function, S. The double lines represent Wilson lines in the fundamental representation and the arrows denote the fermion flow. Every cut propagator corresponds to a real emission. (a) is scaleless and vanishes in dimensional regularization while (b) and its mirror image are the only contributing diagrams since gluons that connect along light-like vectors vanish.

As seen in Chap. 3, all the soft radiation in a $pp \to XL$ process is factorized into a soft function and it is the main goal of this thesis to compute the latter to NNLO. The soft function has been calculated to NLO in Ref. [8] and we will reproduce their results; moreover, the NLO soft function will contribute to NNLO through charge renormalization which requires a higher order expansion in ϵ and η than necessary for NLO. We will calculate it in the fundamental representation. Using Casimir scaling, one can afterwards obtain the result for the soft function in the adjoint representation as well.

The soft function is the vacuum expectation value of four soft Wilson line operators. We can organize the computation in momentum space in so called cut diagrams. Inserting a complete set of states in the matrix element we can express the soft function as

$$S(\mathbf{p}_\perp) = \frac{1}{N_c} \sum\!\!\!\!\!\!\int_X \mathrm{Tr} \left\langle 0 \right| \bar{T} \left[S_n^\dagger S_{\bar{n}} \right] \frac{1}{\pi} \delta(\mathbf{p}_\perp^2 - \mathcal{P}_\perp^2) \left| X \right\rangle \left\langle X \right| T \left[S_{\bar{n}}^\dagger S_n \right] \left| 0 \right\rangle . \tag{4.1}$$

The integration is independent on the azimuthal angle of the transverse plane so we have simplified the measurement function to a one dimensional delta function with the substitution $\delta^{(2)}(\mathbf{p}_\perp - \mathcal{P}_\perp) = \delta(\mathbf{p}_\perp^2 - \mathcal{P}_\perp^2)/\pi$. In our scheme, the transverse integration momentum is always in $2 - 2\epsilon$ dimensions.

To compute S, one simply expands the Wilson lines in α_s; see App. B for a derivation of the Feynman rules. Every contribution can then be represented as a cut diagram, where every cut propagator results in a real emission and gives a factor of an on-shell delta function, $-(2\pi)\delta^+(k^2) \equiv -(2\pi)\theta(k^0)\delta(k^2)$.

4.1 Computation

To the lowest order, S trivially reduces to a simple delta function in momentum space,

$$S(\mathbf{p}_\perp) = \delta^{(2)}(\mathbf{p}_\perp) + \mathcal{O}(\alpha_s). \tag{4.2}$$

The NLO contributions can be organized into pure real emission and pure virtual diagrams, see Fig. 4.1. First we will look closer at the pure virtual diagrams. They are scaleless diagrams that consequently vanish in dimensional regularization. Thus in the end, we are only left with the pure real emission diagrams, which there are two permutations of.

4.1.1 Pure virtual

The pure virtual diagrams contain integrals that does not depend on any dimensionful parameter, hence they are scaleless. That scaleless integrals vanish is a general feature of dimensional regularization. To show it explicitly we compute its integral which is

$$\mathcal{V} \equiv \int d^dk |2k^3|^{-\eta} \frac{1}{(k^- - i\varepsilon)(k^+ + i\varepsilon)(k^2 + i\varepsilon)}. \tag{4.3}$$

We can use the residue theorem to compute the k^0 integral,

$$\begin{aligned}\mathcal{V} &= \int dk^0 \int dk^3 \int d^{d-2}k_\perp |2k^3|^{-\eta} \frac{1}{(k^0 - k^3 - i\varepsilon)(k^0 + k^3 + i\varepsilon)((k^0)^2 - \mathbf{k}^2 + i\varepsilon)} \\ &= -i\pi \int dk^3 \int d^{d-2}k_\perp |2k^3|^{-\eta} \frac{1}{|\mathbf{k}|(|\mathbf{k}| - k^3)k^3}.\end{aligned} \tag{4.4}$$

With the change of variables $x = k^3/|\mathbf{k}_\perp|$ and integrating over the angles this becomes

$$\begin{aligned}\mathcal{V}\Big|_{d=4-2\epsilon} &= -i\pi\Omega_{2-2\epsilon} 2^{-\eta} \int_0^\infty d|\mathbf{k}_\perp| |\mathbf{k}_\perp|^{-1-2\epsilon-\eta} \int_{-\infty}^\infty dx \frac{|x|^{-\eta}}{\sqrt{1+x^2}(\sqrt{1+x^2} - x)x} \\ &= -i\pi\Omega_{2-2\epsilon} 2^{-\eta} \left(\frac{2}{\eta} + \log 4 + \mathcal{O}(\eta)\right) \int_0^\infty d|\mathbf{k}_\perp| |\mathbf{k}_\perp|^{-1-2\epsilon-\eta} \\ &= -i\pi\Omega_{2-2\epsilon} 2^{-\eta} \left(\frac{2}{\eta} + \log 4 + \mathcal{O}(\eta)\right) \left(-\frac{1}{2\epsilon+\eta} + \frac{1}{2\epsilon+\eta}\right) = 0,\end{aligned} \tag{4.5}$$

where the solid angle is $\Omega_d \equiv 2\pi^{d/2}/\Gamma(d/2)$. The parameters ϵ and η need to have different signs in different parts of the integration range for this to converge. But in the end we can use analytic continuation to set them equal in all regions, essentially setting $\epsilon_{\text{IR}} = \epsilon_{\text{UV}}$. With this equality, the diagram vanishes and in the future we will set all the dimensionless diagrams to zero.

4.1.2 Single emission

The only contributing diagram at NLO is the one where a single gluon is emitted from one Wilson line to another along the opposite light-cone direction since gluons that propagate along a light-like vector give factors of $n^2 = 0$ and vanish as well. In the end there is only one diagram and its mirror image that need to be computed and summing up the two gives the expression

$$S_{NLO}(\mathbf{p}_\perp) = \frac{2(n\cdot\bar{n})g^2w^2\nu^\eta\mu^{2\epsilon}}{\pi}\frac{\mathrm{Tr}(t^at^a)}{N_c}\int\frac{d^dk}{(2\pi)^d}|k^- - k^+|^{-\eta}\frac{(2\pi)\delta^+(k^2)\delta(\mathbf{p}_\perp^2 - \mathbf{k}_\perp^2)}{k^-k^+}. \tag{4.6}$$

Here and in the future we will always hide the $+i\varepsilon$ terms in the propagator when they can be ignored. Because of the analytic regulator that picks out a distinct direction, k^3, one needs to be consistent when using dimensional regularization. We choose to always put the transverse components in $2-2\epsilon$ dimensions. The result is

$$\begin{aligned} S_{NLO}(\mathbf{p}_\perp) &= \frac{8C_F\alpha_s w^2\nu^\eta\mu^{2\epsilon}}{(2\pi)^{d-1}}\int_{-\infty}^{\infty}dk^-\int_{-k^-}^{\infty}dk^+|k^- - k^+|^{-\eta}\Omega_{d-2} \\ &\quad\times\int_0^\infty d|\mathbf{k}_\perp||\mathbf{k}_\perp|^{d-3}\frac{\delta(k^+k^- - \mathbf{k}_\perp^2)}{k^-k^+}\frac{\delta(|\mathbf{k}_\perp| - |\mathbf{p}_\perp|)}{2k_\perp}\Big|_{d=4-2\epsilon} \\ &= \frac{8C_F\alpha_s w^2\nu^\eta\mu^{2\epsilon}}{(2\pi)^{3-2\epsilon}}\frac{\Omega_{2-2\epsilon}}{2}(\mathbf{p}_\perp^2)^{-1-\epsilon}\int_0^\infty dk^-\left|k^- - \frac{\mathbf{p}_\perp^2}{k^-}\right|^{-\eta}\frac{1}{k^-}. \end{aligned} \tag{4.7}$$

The last integral is precisely the kind of divergent rapidity integral that was mentioned in Sec. 3.3; now, we can do the integral with the rapidity regulator and find

$$S_{NLO}(\mathbf{p}_\perp) = \frac{8C_F\alpha_s w^2\nu^\eta\mu^{2\epsilon}}{(2\pi)^{3-2\epsilon}}\frac{2\pi^{1-\epsilon}}{2\Gamma(1-\epsilon)}\frac{1}{(\mathbf{p}_\perp^2)^{1+\epsilon+\eta/2}}\frac{\Gamma(\frac{1}{2}-\frac{\eta}{2})\Gamma(\frac{\eta}{2})}{2^\eta\sqrt{\pi}}. \tag{4.8}$$

4.2 Expansion

The bare soft function contains divergences both in ϵ and η. To renormalize it, we need to expand the bare result in Eq. (4.8) in ϵ and η; however, in which order to take their limit to zero is of crucial importance. Since the rapidity divergences arise on the mass hyperbola of $\mathrm{SCET_{II}}$ we need to remain on the hyperbola when we take the rapidity cut-off to its limit. Thus we take the $\eta \to 0$ limit before $\epsilon \to 0$ with $\eta/\epsilon^n \to 0, \forall n > 0$. Moreover, care must be taken when doing so to avoid getting factors like $\delta^{(2)}(\mathbf{p}_\perp)\log(\mathbf{p}_\perp^2/\mu^2)$ which are ill-defined and a proper way of doing everything is to make use of plus distributions that regulate the divergences at $\mathbf{p}_\perp^2 = 0$. Details about plus distributions can be found in App. C and throughout this thesis we will make use of a certain class of plus distributions which we define to be

$$\mathcal{L}_n(\mathbf{p}^2,\mu^2) = \frac{1}{2\pi\mu^2}\left[\frac{\mu^2}{\mathbf{p}^2}\log^n\left(\frac{\mu^2}{\mathbf{p}^2}\right)\right]_+. \tag{4.9}$$

We also need to include the $\overline{\mathrm{MS}}$ factor and the renormalization of α_s. This is done by the following replacement in the bare function

$$\alpha_s^b\mu^{2\epsilon} \to \mu^{2\epsilon}\alpha_s(\mu)\frac{e^{\epsilon\gamma_E}}{(4\pi)^\epsilon}\left(1 - \beta_0\frac{\alpha_s}{4\pi}\frac{1}{\epsilon} + \mathcal{O}(\alpha_s^2)\right). \tag{4.10}$$

From this it is clear that the NLO result contributes to NNLO. In addition we will see in Sec. 5.3 that by using the non-abelian exponentiation theorem, we can get the total C_F^2 part of the soft function from the NLO result. The exact relation is a convolution of two NLO renormalized soft functions in momentum space, see Eq. (5.47). One needs to be careful when expanding S_{NLO} because of this and additional convolutions in the renormalization procedure. In order not to miss any non-zero terms, S_{NLO} needs to be expanded all the way up to and including $\mathcal{O}(\eta)$ and $\mathcal{O}(\epsilon^4)$, for NNLO.

Now when expanding Eq. (4.8), we first write out $1/(\mathbf{p}_\perp^2)^{1+\frac{\eta}{2}+\epsilon}$ as a series of plus distributions with Eq. (C.6). Since the full expansion that is needed is rather lengthy, we only show the derivation of the divergent and finite terms to first order in α_s as an example of the method. The plus distribution series is then

$$\begin{aligned}\frac{1}{(\mathbf{p}_\perp^2)^{1+\frac{\eta}{2}+\epsilon}} &= \mu^{-2-2\epsilon-\eta}\left(\frac{\mu^2}{\mathbf{p}_\perp^2}\right)^{1+\epsilon+\eta/2} = \mu^{-2\epsilon-\eta}\left(-\frac{\pi\delta^{(2)}(\mathbf{p}_\perp)}{\epsilon+\eta/2} + 2\pi\sum_{n=0}^{\infty}\frac{(\epsilon+\eta/2)^n}{n!}\mathcal{L}_n\right)\\ &= \mu^{-2\epsilon-\eta}\left[-\frac{\pi\delta^{(2)}(\mathbf{p}_\perp)}{\epsilon} + \left(\frac{\pi\delta^{(2)}(\mathbf{p}_\perp)}{2\epsilon^2} + \pi\eta\mathcal{L}_1\right)\eta\right] + \mathcal{O}(\eta^2) + \mathcal{O}(\epsilon). \quad (4.11)\end{aligned}$$

Inserting this in Eq. (4.8) gives the final bare NLO result

$$\begin{aligned}S_{NLO}(\mathbf{p}_\perp) = \alpha_s C_F w^2\Bigg[&\frac{\delta^{(2)}(\mathbf{p}_\perp)}{\pi}\left(\frac{1}{\epsilon^2}+\frac{1}{\epsilon}\log\frac{\mu}{\nu}\right) + \frac{1}{\eta}\left(-\frac{2}{\pi\epsilon}\delta^{(2)}(\mathbf{p}_\perp) + \frac{4}{\pi}\mathcal{L}_0\right)\\ &-\frac{\pi\delta^{(2)}(\mathbf{p}_\perp)}{12} - \frac{4}{\pi}\mathcal{L}_0\log\frac{\mu}{\nu} + \frac{2}{\pi}\mathcal{L}_1\Bigg] + \mathcal{O}(\eta) + \mathcal{O}(\epsilon). \quad (4.12)\end{aligned}$$

This agrees with the computation of the NLO soft function in Ref. [8][1].

[1] Up to potential typos in their article. They compute it in the adjoint representation, which translates to the fundamental if one substitute C_F for C_A. However, they are missing the w^2 factor as well as a factor of π in the finite $\delta^{(2)}(\mathbf{p}_\perp)$ term, compared to our result.

Chapter 5

Soft Function at NNLO

The number of diagrams in a computation increases rapidly for every order. At NNLO we will divide them into different groups that we will compute separately with different techniques. As in the NLO case, we do not compute any purely scaleless diagrams. The simplest non-trivial diagrams have a single real gluon and will be denoted by $\mathcal{R}$, see Fig. 5.1. We will use the non-abelian exponentiation theorem as well as the known soft current at one loop to compute them.

For the more involved case with two real particles we will develop a calculation scheme which can be applied to all diagrams. They will be divided into five groups that we compute separately for convenience.

The color structure of all the diagrams can be seen in Tab. 5.1.

Color Factor	Diagrams
C_F	(NLO)
C_F^2	$\mathcal{I}$ and $\mathcal{R}$
$C_F C_A$	$\mathcal{I}$, $\mathcal{T}$, $\mathcal{G}$, $\mathcal{H}$ and $\mathcal{R}$
$C_F T_F n_f$	$\mathcal{Q}$

Table 5.1: The diagrams that contain the respective color factor. All of the diagrams are collected in Fig. 4.1, 5.1 and 5.2. After renormalization, the NLO diagram contributes to both $C_F C_A$ and $C_F T_F n_f$ through the α_s beta function; moreover, we will use the NLO results to get the full C_F^2 part of the soft function by using the non-abelian exponentiation theorem.

5.1 Single Real Emission

Two types of single real emission diagrams are shown in Fig. 5.1 and we will denote all permutations of them as $\mathcal{R}$. The non-abelian exponentiation theorem states that the total C_F^2 term of the soft function can be retrieved by squaring the C_F term, i.e. the NLO result [23, 24]. Thus the C_F^2 part of both the single and double emission diagrams will therefore not be considered any further. See Sec. 5.3 for the computation of the C_F^2 part.

For the $C_F C_A$ part of the $\mathcal{R}$ diagrams we will use the known soft current at one loop, which we can extract from [25]. In the end it only results in an overall factor multiplied

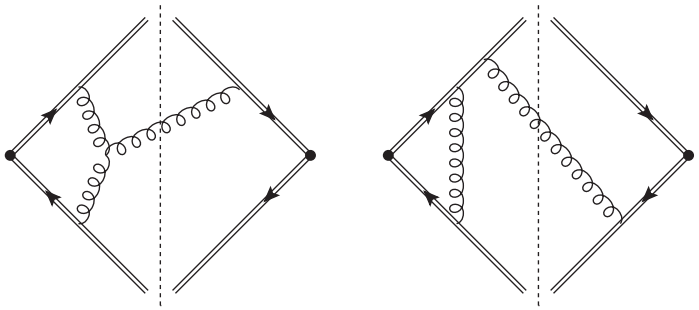

(a) (b)

Figure 5.1: The simplest diagrams at NNLO are the ones with a single real gluon. Their sum is denoted by $\mathcal{R}$. We will compute them with the non-abelian exponentiation theorem as well as the known 1-loop soft current.

by the bare NLO diagram. It is evaluated to

$$\begin{aligned}\mathcal{R}_{C_F C_A} &= -2^{-1-2\epsilon}\pi^{-1+\epsilon}\alpha_s\mu^{2\epsilon}C_A\frac{\Gamma(1-\epsilon)^4\Gamma(1+\epsilon)^3}{\epsilon^2\Gamma(1-2\epsilon)^2\Gamma(1+2\epsilon)}\frac{4C_F(4\pi)\alpha_s w^2\nu^\eta\mu^{2\epsilon}}{\pi} \\ &\quad\times\int\frac{d^dk}{(2\pi)^d}|k^- - k^+|^{-\eta}\frac{(2\pi)\delta^+(k^2)\delta(\mathbf{p}_\perp^2-\mathbf{k}_\perp^2)}{(k^-k^+)^{1+\epsilon}}\Big|_{d=4-2\epsilon} \\ &= -\alpha_s^2 C_F C_A w^2\pi^{2\epsilon-\frac{7}{2}}2^{-\eta+4\epsilon-1}\mu^{4\epsilon}\nu^\eta\frac{\Gamma(\frac{1}{2}-\frac{\eta}{2})\Gamma(\frac{\eta}{2})\Gamma(1-\epsilon)^3\Gamma(1+\epsilon)^3}{\epsilon^2\Gamma(1-2\epsilon)^2\Gamma(1+2\epsilon)}\frac{1}{(\mathbf{p}_\perp^2)^{1+2\epsilon+\frac{\eta}{2}}}. \end{aligned} \tag{5.1}$$

5.2 Double Real Emission

The diagrams with two real particles emitted are shown in Fig. 5.2; they are the most complicated cases that need to be calculated. We will introduce a parametrization scheme similar to that used in Ref. [12] and [26]. This will result in a master integral that will allow us to express all these diagrams in a closed form with the help of Hypergeometric functions.

The double emission diagrams have two integrals, one over each real particle momentum k_1 and k_2. However, due to our regulator and measurement, we find it useful to use the variables $\ell = k_1$ and $k = k_1 + k_2$. Then the integral that needs to be performed takes the form

$$I_{RR} \equiv 4\pi\int\frac{d^d\ell}{(2\pi)^d}\int\frac{d^dk}{(2\pi)^d}|k^- - k^+|^{-\eta}\delta^+(\ell^2)\delta^+\left((k-\ell)^2\right)\delta(\mathbf{p}_\perp^2-\mathbf{k}_\perp^2)\mathcal{A}(\ell,k,k\cdot\ell). \tag{5.2}$$

The factor of 4π in front comes from the two cut propagators and the measurement function. All the amplitudes of the diagrams in Fig. 5.2 can be found in Ref. [27].

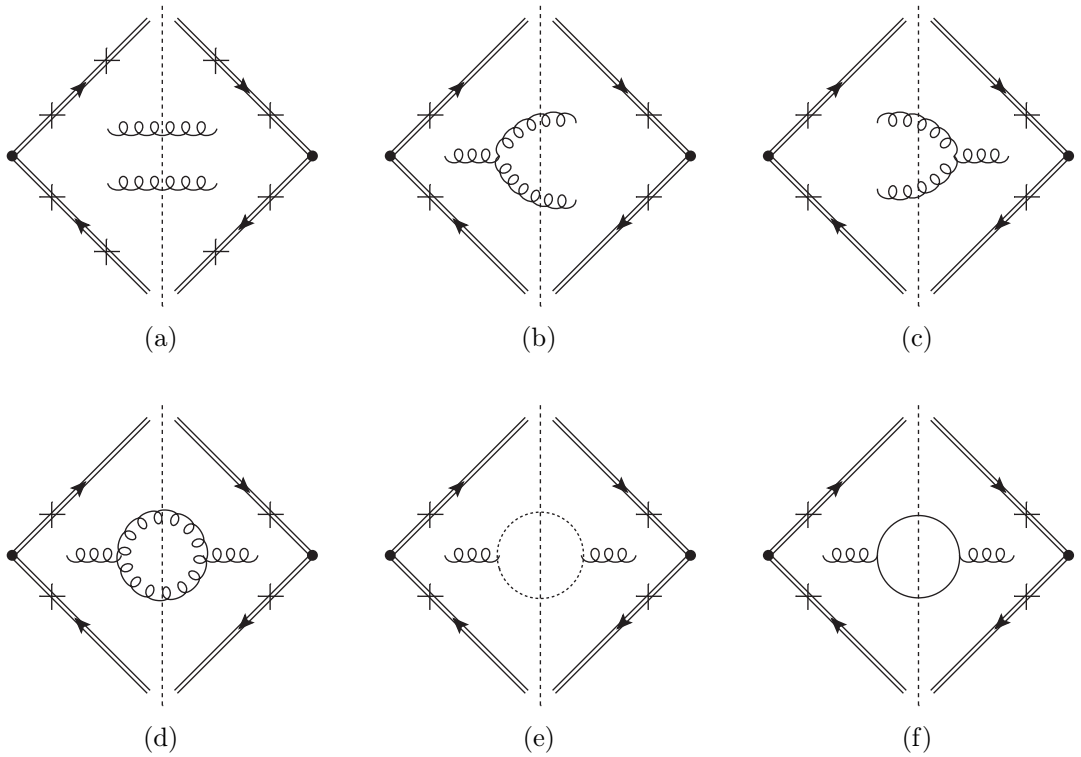

Figure 5.2: All the double real emission diagrams contributing at NNLO. The free gluons can connect to any of the + points on their side of the cut. We divide them into five groups: three double gluon groups $\mathcal{I}$: (a), $\mathcal{T}$: (b) & (c) and $\mathcal{G}$: (d); one with ghosts $\mathcal{H}$: (e); and one with fermions $\mathcal{Q}$: (f)

5.2.1 Kinematics and parameterization

From the delta functions we now have the on-shell condition on ℓ and $(k-\ell)$ which implies that

$$\begin{aligned} \ell^2 &= 0, & (k-\ell)^2 &= 0, \\ \ell^0 &\geq 0, & (k-\ell)^0 &\geq 0. \end{aligned} \tag{5.3}$$

In the center-of-mass frame of the two particles, where

$$k^\mu = (k^0, 0, 0, 0), \tag{5.4}$$

we have $\frac{1}{2}k^0 = \ell^0 \geq 0$, which implies $k^2 \geq 0$. Given that the zero components of n and $\bar{n}$ are positive we can conclude that we have

$$k^+ \geq 0, \tag{5.5}$$
$$k^- \geq 0, \tag{5.6}$$

in any frame. In evaluating the k integral in Eq. (5.2) we find a set of convenient variables to be

$$y = \frac{\mathbf{k}_\perp^2}{k^- k^+} \geq 0, \tag{5.7}$$
$$v = k^- - k^+. \tag{5.8}$$

The integration over the light-cone components then takes the form

$$\int dk^0 \int dk^3 = \frac{1}{2}\int_0^\infty dk^- \int_{\mathbf{k}_\perp^2/k^-}^\infty dk^+ = \int_0^1 dy \int_{-\infty}^\infty dv|J|, \tag{5.9}$$

where the Jacobian is

$$|J| = \frac{\mathbf{k}_\perp^2}{y^{3/2}\sqrt{yv^2+4\mathbf{k}_\perp^2}}. \tag{5.10}$$

We will see in sections below that nothing else except the regulator factor $|v|^{-\eta}$ is dependent on the variable v. This is the major advantage of our choice of variables, because now we can compute the v integral independently. It evaluates to

$$\int_{-\infty}^\infty dv|J||v|^{-\eta} = \int_{-\infty}^\infty dv \frac{\mathbf{k}_\perp^2}{y^{3/2}\sqrt{yv^2+4\mathbf{k}_\perp^2}}|v|^{-\eta} = 2^{-\eta}(\mathbf{k}_\perp^2)^{1-\frac{\eta}{2}} y^{-2+\frac{\eta}{2}}\beta\left(\frac{1-\eta}{2},\frac{\eta}{2}\right). \tag{5.11}$$

The y and $\mathbf{k}_\perp$ integral receives contributions from the ℓ integral, which we consider next.

The ℓ integration in Eq. (5.2) has the form

$$\int d^d\ell \delta^+(\ell^2)\delta^+\left((k-\ell)^2\right)\mathcal{A}(\ell,k,k\cdot\ell). \tag{5.12}$$

The amplitude is a function of the scalar product of ℓ and k with the light-cone vectors n and $\bar{n}$; as well as $\ell\cdot k$. We are free to rotate the coordinate system of ℓ with respect to k as we like and we can thus set up k in the most convenient reference frame. The center-of-mass frame of k which we discussed earlier is clearly the simplest choice. Thus we parametrize k as

$$k^\mu = |\mathbf{k}_\perp|\sqrt{\frac{1-y}{y}}(1,0,0,0). \tag{5.13}$$

The momenta k and ℓ are vectors in d dimensions. Here, we will put the k^1 and ℓ^1 components in $d-3$ dimensions. After going to the center of mass frame, there still remains freedom in rotating in $d-1$ dimensions. The ℓ vector will be expressed in terms of d dimensional spherical coordinates and the next step is to choose a parameterization of n and $\bar{n}$ in terms of k components with as many zero components as possible. We start by setting up $\bar{n}$ such that it only has two components. Then, n can be rotated in the remaining plane and will contain three components. This is parametrized as

$$\begin{aligned}\bar{n}^\mu &= c_{\bar{n}}(1,\ldots,0,x_3),\\ n^\mu &= c_n(1,\ldots,y_2,y_3),\\ \ell^\mu &= c_\ell(z_0,\ldots,\sin\theta_1\cos\theta_2,\cos\theta_1),\end{aligned} \tag{5.14}$$

where the dots denotes the components of a $d-3$ vector in spherical coordinates. To fix

all these 7 coefficients we will apply the conditions

$$\begin{aligned}
\ell^0 &= \frac{|\mathbf{k}_\perp|}{2}\sqrt{\frac{1-y}{y}},\\
\bar{n}\cdot\bar{n} &= n\cdot n = \ell\cdot\ell = 0,\\
\bar{n}\cdot n &= 2,\\
\bar{n}\cdot k = k^- &= \frac{1}{2}\left(\sqrt{v^2+\frac{4\mathbf{k}_\perp^2}{y}}+v\right),\\
n\cdot k = k^+ &= \frac{1}{2}\left(\sqrt{v^2+\frac{4\mathbf{k}_\perp^2}{y}}-v\right).
\end{aligned} \tag{5.15}$$

Which gives us the vectors

$$\begin{aligned}
\bar{n} &= \frac{k^-}{|\mathbf{k}_\perp|}\sqrt{\frac{y}{1-y}}(1,\dots,0,1),\\
n &= \frac{|\mathbf{k}_\perp|}{k^-}\frac{1}{\sqrt{y(1-y)}}(1,\dots,-2\sqrt{y(1-y)},2y-1),\\
\ell &= \frac{|\mathbf{k}_\perp|}{2}\sqrt{\frac{1-y}{y}}(1,\dots,\sin\theta_1\cos\theta_2,\cos\theta_1).
\end{aligned} \tag{5.16}$$

Now we can express the amplitude in terms of $|\mathbf{k}_\perp|$, k^- and y, as well as the angles θ_1, θ_2 and θ_3. All angle dependent factors that can appear in the amplitudes are now

$$\begin{aligned}
\bar{n}\cdot\ell &= k^- D_1, & n\cdot\ell &= \frac{\mathbf{k}_\perp^2}{k^- y}D_2,\\
\bar{n}\cdot(k-\ell) &= k^- D_3, & n\cdot(k-\ell) &= \frac{\mathbf{k}_\perp^2}{k^- y}D_4,
\end{aligned} \tag{5.17}$$

where we have defined the following functions

$$\begin{aligned}
D_1 &= \frac{1-\cos\theta_1}{2},\\
D_2 &= \frac{1}{2}\left(1+2\sqrt{y(1-y)}\sin\theta_1\cos\theta_2+(2y-1)\cos\theta_1\right),\\
D_3 &= 1-D_1,\\
D_4 &= 1-D_2.
\end{aligned} \tag{5.18}$$

Note that none of these factors depend on the $d-3$ spherical coordinates. It is also convenient to define

$$\begin{aligned}
D_5 &= y,\\
D_6 &= 1-y.
\end{aligned} \tag{5.19}$$

All the double real emission amplitudes can be expressed in terms of these D_i-factors. The $\mathbf{k}_\perp$ can be factored out and the amplitudes can be written as

$$\mathcal{A}(k,\ell,k\cdot\ell) = \frac{1}{\mathbf{k}_\perp^4}\tilde{\mathcal{A}}\left(\{D_i\}\right) \tag{5.20}$$

The whole computation of Eq. (5.2) factorizes nicely and we can do the ℓ and y integrals independently from the v and $\mathbf{k}_\perp$ integrals.

5.2.2 The ℓ and y integrals

We can now perform two integrals in Eq. (5.12) with the help of the delta functions which reduces them to

$$\int d^d\ell\delta^+(\ell^2)\delta^+\left((k-\ell)^2\right) = \int d\ell^0 \frac{1}{2k^0}\delta(\ell^0 - \frac{1}{2}k^0)\int d|\ell||\ell|^{d-2}\frac{1}{2|\ell|}\delta(|\ell| - \ell^0)\int d\Omega_{d-1}$$
$$= 2^{-3+2\epsilon}(k^0)^{-2\epsilon}\int_0^\pi d\theta_1 \sin^{1-2\epsilon}\theta_1 \int_0^\pi d\theta_2 \sin^{-2\epsilon}\theta_2 \int d\Omega_{d-3}. \quad (5.21)$$

The fact that nothing depends on the $d-3$ angular components lets us do the last integral straight away. After substituting $(k^0)^2 = k^2 = \mathbf{k}_\perp^2 \frac{1-y}{y} = \mathbf{k}_\perp^2 D_5^{-1} D_6$ and going to $d = 4-2\epsilon$ we get

$$2^{-2}(\pi\mathbf{k}_\perp^2)^{-\epsilon} D_5^\epsilon D_6^{-\epsilon}\frac{\Gamma(1-\epsilon)}{\Gamma(1-2\epsilon)}\int_0^\pi d\theta_1 \sin^{1-2\epsilon}\theta_1 \int_0^\pi d\theta_2 \sin^{-2\epsilon}\theta_2. \quad (5.22)$$

We will find it useful to define a main integral over the remaining angles as well as the integral over y in Eq. (5.9). Thus we define

$$I(a_1,a_2,a_3,a_4,a_5,a_6) = \int_0^1 dy \frac{1}{2\pi}\frac{\Gamma^2(1-\epsilon)}{\Gamma(1-2\epsilon)}\int_0^\pi d\theta_1 \sin^{1-2\epsilon}\theta_1 \int_0^\pi d\theta_2 \sin^{-2\epsilon}\theta_2 \prod_{i=1}^6 D_i^{-a_i}. \quad (5.23)$$

The arbitrary factors are only there for convenience to avoid certain γ_E factors when expanding. This integral will in the end act as the master formula that can express all amplitudes in terms of Hypergeometric functions.

5.2.3 The I integral

Here we will compute the I integral in Eq. (5.23). Before computing it we can pause to consider some of its properties that are useful when one wants to express amplitudes in terms of it.

Relabeling

In our parameterization of the light-cone vectors n and $\bar{n}$ we could have just as well switched one for the other. This leads to an identity for our I-integral where we can relabel it as follows:

$$I(a_1,a_2,a_3,a_4,a_5,a_6) = I(a_2,a_1,a_4,a_3,a_5,a_6). \quad (5.24)$$

The fact that our initial choice of setting $\ell = k_1$ was arbitrary and symmetrical to setting $\ell = k_2$ leads in a similar way to

$$I(a_1,a_2,a_3,a_4,a_5,a_6) = I(a_3,a_4,a_1,a_2,a_5,a_6). \quad (5.25)$$

These relations are very useful to minimize the number of terms in the computation when matching the amplitudes to the I integrals.

Evaluation

To simplify the computation of I, we first split it up like

$$I(a_1,a_2,a_3,a_4,a_5,a_6) = \int_0^1 dy y^{-a_5}(1-y)^{-a_6} I_1(a_1,a_2,a_3,a_4), \tag{5.26}$$

where

$$I_1(a_1,a_2,a_3,a_4) = \frac{1}{2\pi}\frac{\Gamma^2(1-\epsilon)}{\Gamma(1-2\epsilon)}\int_0^\pi d\theta_1 \sin^{1-2\epsilon}\theta_1 \int_0^\pi d\theta_2 \sin^{-2\epsilon}\theta_2 D_1^{-a_1} D_2^{-a_2} D_3^{-a_3} D_4^{-a_4}. \tag{5.27}$$

Note however that I_1 depends on y, through D_2 and D_4, and must be integrated over. When writing down the amplitudes we can use partial fraction decomposition such that two of the indices in I_1 are zero. This has a convenient consequence, because by relabeling the indices we can freely choose such that we only need to compute integrals with $a_4 = 0$. Hence, in total there are three combinations of possible non-zero indices.

The simplest combination is when $a_2 = a_4 = 0$, since in that case I_1 does not depend on y. Then I_1 evaluates to

$$I_1(a_1,0,a_3,0) = \frac{\Gamma(1-\epsilon-a_1)\Gamma(1-\epsilon-a_2)}{\Gamma(2-2\epsilon-a_1-a_3)} \tag{5.28}$$

and the final expression for I is simply a collection of gamma functions,

$$I(a_1,0,a_3,0,a_5,a_6) = \frac{\Gamma(1-a_5)\Gamma(1-a_6)}{\Gamma(2-a_3-a_6)}\frac{\Gamma(1-\epsilon-a_1)\Gamma(1-\epsilon-a_2)}{\Gamma(2-2\epsilon-a_1-a_3)}. \tag{5.29}$$

For the other cases we find

$$I_1(a_1,a_2,0,0) = \frac{\Gamma(1-\epsilon-a_1)\Gamma(1-\epsilon-a_2)}{\Gamma(2-2\epsilon-a_1-a_2)} {}_2F_1(a_1,a_2;1-\epsilon;y), \tag{5.30}$$

$$I_1(0,a_2,a_3,0) = \frac{\Gamma(1-\epsilon-a_2)\Gamma(1-\epsilon-a_3)}{\Gamma(2-2\epsilon-a_2-a_3)} {}_2F_1(a_2,a_3;1-\epsilon;1-y). \tag{5.31}$$

Some relevant details about Hypergeometric functions can be found in App. D and by using the integral representation in Eq. (D.6), we can do the last remaining integral over y to get a final closed form in terms of a ${}_3F_2$ function. However, one needs to be careful about singularities in the ${}_2F_1(a,b;c;z)$ when integrating over it. When $-1 < c-a-b \leq 0$, the ${}_2F_1$ diverges at $z=1$ which is inside the integration range. Naively applying the integral representation then gives a divergent ${}_3F_2$. Instead, one can extract the singularity with the Euler transformation in Eq. (D.5) before integrating over y, to yield a well behaved ${}_3F_2$. By doing this, we end up with

$$\begin{aligned} I(a_1,a_2,0,0,a_5,a_6) =& \frac{\Gamma(1-\epsilon-a_1)\Gamma(1-\epsilon-a_2)}{\Gamma(2-a_1-a_2-2\epsilon)}\frac{\Gamma(1-a_5)\Gamma(2-a_1-a_2-a_6-\epsilon)}{\Gamma(3-a_1-a_2-a_5-a_6-\epsilon)} \\ &\times {}_3F_2\left(\begin{matrix}1-a_5, 1-\epsilon-a_1, 1-\epsilon-a_2 \\ 3-a_1-a_2-a_5-a_6-\epsilon, 1-\epsilon\end{matrix};1\right), \end{aligned} \tag{5.32}$$

$$\begin{aligned} I(0,a_2,a_3,0,a_5,a_6) =& \frac{\Gamma(1-\epsilon-a_2)\Gamma(1-\epsilon-a_3)}{\Gamma(2-a_2-a_3-2\epsilon)}\frac{\Gamma(1-a_6)\Gamma(2-a_2-a_3-a_5-\epsilon)}{\Gamma(3-a_1-a_2-a_5-a_6-\epsilon)} \\ &\times {}_3F_2\left(\begin{matrix}1-a_6, 1-\epsilon-a_2, 1-\epsilon-a_3 \\ 3-a_2-a_3-a_5-a_6-\epsilon, 1-\epsilon\end{matrix};1\right). \end{aligned} \tag{5.33}$$

5.2.4 The $\mathbf{k}_\perp$ integral

The integral over $\mathbf{k}_\perp$ is the only remaining integral to do. First note that all the amplitudes are proportional to $(\mathbf{k}_\perp^2)^{-2}$, but we also pick up additional factors. A factor of $(\mathbf{k}_\perp^2)^{1-\frac{\eta}{2}}$ from the v integral in Eq. (5.11) and a factor $(\mathbf{k}_\perp^2)^{-\epsilon}$ from the angle integrations, see Eq. (5.22). In the end we are left with the following integral which is easily evaluated with the standard dimensional regularization technique:

$$\begin{aligned}\int d^{d-2}\mathbf{k}_\perp(\mathbf{k}_\perp^2)^{-1-\epsilon-\frac{\eta}{2}}\delta(\mathbf{p}_\perp^2-\mathbf{k}_\perp^2) &= \frac{\Omega_{d-2}}{2}\int_0^\infty d|\mathbf{k}_\perp||\mathbf{k}_\perp|^{d-5-2\epsilon-\eta}\delta(|\mathbf{p}_\perp|-|\mathbf{k}_\perp|)\\ &= \frac{\Omega_{d-2}}{2}\frac{1}{(\mathbf{p}_\perp^2)^{-\frac{d}{2}+\frac{5}{2}+\epsilon+\frac{\eta}{2}}}\Big|_{d=4-2\epsilon} = \frac{\pi^{1-\epsilon}}{\Gamma(1-\epsilon)}\frac{1}{(\mathbf{p}_\perp^2)^{1+2\epsilon+\frac{\eta}{2}}}. \quad (5.34)\end{aligned}$$

5.2.5 Final form

In previous sections we have seen that the computation of the double real emission diagrams in the end results in a closed expression. All diagrams can be divided into separate groups for convenience but they all share the same fundamental 2-loop integral. The integrals factorize nicely though. By first using the two on-shell delta functions, one can reduce the integral over one momentum ℓ to an integration over 2 angles. These can then be combined with one integral of the k components to get a master formula that evaluates to Hypergeometric functions. Another component of the k momentum can also be done independently and finally there is the $2-2\epsilon$ integral over $\mathbf{k}_\perp$ which is trivially done with the help of the measurement delta function. In the end, the full I_{RR} integral takes the form

$$I_{RR} = \frac{2^{-9+4\epsilon-\eta}\pi^{-6+2\epsilon}}{\Gamma^2(1-\epsilon)}\beta\left(\frac{1-\eta}{2},\frac{\eta}{2}\right)\frac{1}{(\mathbf{p}_\perp^2)^{1+2\epsilon+\frac{\eta}{2}}}I_{y\theta_1\theta_2}, \quad (5.35)$$

where each term in

$$I_{y\theta_1\theta_2} \equiv \int_0^1 dy\frac{1}{2\pi}\frac{\Gamma^2(1-\epsilon)}{\Gamma(1-2\epsilon)}\int_0^\pi d\theta_1\sin^{1-2\epsilon}\theta_1\int_0^\pi d\theta_2\sin^{-2\epsilon}\theta_2 D_5^{-2+\epsilon+\eta/2}D_6^{-\epsilon}\tilde{\mathcal{A}}(\{D_i\}) \quad (5.36)$$

can be matched onto the I integrals in Eq. (5.23) and $\tilde{\mathcal{A}}$ is defined by Eq. (5.20).

The amplitudes for the double real emission diagrams in Fig. 5.2 can be found in Ref. [27]. Here, we express them in terms of the D_i factors that are defined in Sec. 5.2.1. Some terms between the ghost and gluon loop diagrams cancel so we add them together. We also split the $\mathcal{I}$ diagrams into distinct color factors. All the double real emission

amplitudes are in Feynman gauge

$$\mathcal{A}_{\mathcal{I}_{C_F C_A}} = \frac{1}{\mathbf{k}_\perp^4}\left(-2(4\pi^2)\alpha^2\mu^{4\epsilon}\nu^\eta w^2 C_F C_A\right) D_5^2\left(3D_1^{-1}D_2^{-1}+2D_2^{-1}D_3^{-1}+D_3^{-1}D_4^{-1}\right), \quad (5.37)$$

$$\begin{aligned}\mathcal{A}_{\mathcal{T}} =& \frac{1}{\mathbf{k}_\perp^4}\left(2(4\pi)^2\alpha^2\mu^{4\epsilon}\nu^\eta w^2 C_F C_A\right) D_5^2 D_6^{-1} \\ &\times\left(D_1 D_3^{-1}+D_2^{-1}D_3^{-1}+D_1^{-1}D_3+D_1^{-1}D_4^{-1}+D_2 D_4^{-1}+D_2^{-1}D_4\right), \end{aligned} \quad (5.38)$$

$$\begin{aligned}\mathcal{A}_{\mathcal{G}+\mathcal{H}} =& \frac{1}{\mathbf{k}_\perp^4}\left[(4\pi^2)\alpha^2\mu^{4\epsilon}\nu^\eta w^2 C_F C_A\right] D_5^2 D_6^{-2} \\ &\times\left(4D_1^2-8D_1D_2+4D_2^2-8D_6-4D_1^2\epsilon+8D_1D_2\epsilon-4D_2^2\epsilon\right)\end{aligned} \quad (5.39)$$

$$\mathcal{A}_{\mathcal{Q}} = \frac{1}{\mathbf{k}_\perp^4}\left(8(4\pi^2)\alpha^2\mu^{4\epsilon}\nu^\eta w^2 T_F n_f C_F\right) D_5^2 D_6^{-2}\left(-D_1^2+2D_1D_2-D_2^2+D_6\right). \quad (5.40)$$

5.2.6 Results

After plugging the amplitudes into Eq. (5.35) and matching onto the I integrals, the double real emission diagrams are evaluated to

$$\mathcal{I}_{C_F C_A} = 4C_F C_A K_{\rm RR}\left[3I(1,1,0,0,-\epsilon-\frac{\eta}{2},\epsilon)+2I(0,1,1,0,-\epsilon-\frac{\eta}{2},\epsilon)\right], \quad (5.41)$$

$$\mathcal{T} = 4C_F C_A K_{\rm RR}\left[2I(-1,0,1,0,-\epsilon-\frac{\eta}{2},1+\epsilon)+I(0,1,1,0,-\epsilon-\frac{\eta}{2},1+\epsilon)\right], \quad (5.42)$$

$$\begin{aligned}\mathcal{G}+\mathcal{H} =& 4C_F C_A K_{\rm RR}\Big[I(-2,0,0,0,-\epsilon-\frac{\eta}{2},2+\epsilon)-2I(-1,-1,0,0,-\epsilon-\frac{\eta}{2},2+\epsilon) \\ &+I(0,-2,0,0,-\epsilon-\frac{\eta}{2},2+\epsilon)-2I(0,0,0,0,-\epsilon-\frac{\eta}{2},1+\epsilon) \\ &-\epsilon I(-2,0,0,0,-\epsilon-\frac{\eta}{2},2+\epsilon)+2\epsilon I(-1,-1,0,0,-\epsilon-\frac{\eta}{2},2+\epsilon) \\ &-\epsilon I(0,-2,0,0,-\epsilon-\frac{\eta}{2},2+\epsilon)\Big],\end{aligned} \quad (5.43)$$

$$\begin{aligned}\mathcal{Q} =& 8C_F T_F n_f K_{\rm RR}\Big[-I(-2,0,0,0,-\epsilon-\frac{\eta}{2},2+\epsilon)+2I(-1,-1,0,0,-\epsilon-\frac{\eta}{2},2+\epsilon) \\ &-I(0,-2,0,0,-\epsilon-\frac{\eta}{2},2+\epsilon)+I(0,0,0,0,-\epsilon-\frac{\eta}{2},1+\epsilon)\Big],\end{aligned} \quad (5.44)$$

where the common prefactor is

$$K_{\rm RR} = \frac{2^{-4+4\epsilon-\eta}\pi^{-3+2\epsilon}\alpha_s^2\mu^{4\epsilon}\nu^\eta w^2\beta(\frac{1-\eta}{2},\frac{\eta}{2})}{\Gamma(1-\epsilon)^2}\frac{1}{(\mathbf{p}_\perp^2)^{1+2\epsilon+\frac{\eta}{2}}}. \quad (5.45)$$

5.3 Non-Abelian Exponentiation Theorem

Throughout the previous calculations of diagrams we have neglected any C_F^2 pieces. We will instead retrieve these terms through the non-abelian exponentiation theorem [23, 24]. We discussed this briefly in Sec. 3.3.1 and according to this theorem the soft function can be written as an exponential of C-Webs in position space. The C-Webs are sets of diagrams at a certain order in α_s and each C-Web carries a distinct color factor. We

write this exponent as

$$S(\alpha_s) = \frac{1}{(2\pi)^2}\exp\left[\sum_{n=1}^{\infty} s^{(n)}\left(\frac{\alpha_s}{4\pi}\right)^n\right] = \frac{1}{(2\pi)^2}\left[1 + s^{(1)}\left(\frac{\alpha_s}{4\pi}\right) + \left(\frac{1}{2}(s^{(1)})^2 + s^{(2)}\right)\left(\frac{\alpha_s}{4\pi}\right)^2 + \mathcal{O}(\alpha_s^3)\right], \tag{5.46}$$

The factor of $1/(2\pi)^2$ is a normalization factor. Here, we can identify the $\mathcal{O}(\alpha_s)$ term as the Fourier transform of S_{NLO}. The non-abelian exponentiation theorem states that the $s^{(1)}$ is purely C_F while $s^{(2)}$ is purely $C_F C_A$ and $C_F n_f$. Hence the total C_F^2 part of the soft function is equal to the $(s^{(1)})^2$ term in Eq. (5.46). We can use this fact and simply square the NLO result to obtain the full C_F^2 part. When we Fourier transform to momentum space the square will turn into a convolution and we get

$$S_{C_F^2}(\mathbf{p}) = \mathcal{F}\left[\frac{1}{(2\pi)^2}\frac{1}{2}s^{(1)}(\mathbf{b})^2\left(\frac{\alpha_s}{4\pi}\right)^2\right] = \frac{(2\pi)^2}{2}S_{NLO}\otimes_\perp S_{NLO}(\mathbf{p}). \tag{5.47}$$

The convolution in momentum space is defined as

$$g\otimes_\perp f \equiv \int \frac{d^2q}{(2\pi)^2} f(\mathbf{q}-\mathbf{p})g(\mathbf{q}). \tag{5.48}$$

We also define a compact notation for the identity in this 2-dimensional space as

$$\mathbb{I}_p \equiv (2\pi)^2\delta^{(2)}(\mathbf{p}). \tag{5.49}$$

Chapter 6

Results

The final results for the bare NNLO soft function can then be collected and written down as

$$S_B = \delta^{(2)}(\mathbf{p}_\perp) + S_{NLO}\left(1 - \beta_0 \frac{\alpha_s}{4\pi}\frac{1}{\epsilon}\right) + \frac{(2\pi)^2}{2} S_{NLO} \otimes_\perp S_{NLO} + \mathcal{R}_{C_F C_A} + \mathcal{I}_{C_F C_A} + \mathcal{T} + \mathcal{G} + \mathcal{H} + \mathcal{Q}, \quad (6.1)$$

where we have introduced the subscript B for bare. From now on we will also use the subscript R for renormalized. The NLO bare result, S_{NLO}, can be found in Eq. (4.8) and in Ref. [8]. The $C_F C_A$ part of the NNLO real-virtual diagrams, $\mathcal{R}_{C_F C_A}$, is written down in Eq. (5.1). As shown in Sec. 5.3, we can use the non-abelian exponentiation theorem to get the C_F^2 part from S_{NLO}, which produces the convolution term. All the double real emission diagrams, $\mathcal{I}_{C_F C_A}, \mathcal{T}, \mathcal{G}, \mathcal{H}$ and $\mathcal{Q}$, are written down in Eq. (5.41)-(5.44).

The bare closed form in d dimensions, though compact, is not very useful and eventually we are interested in the renormalized soft function, i.e. we want to send $\eta \to 0$ and go to $d = 4$. Thus we need to expand all the contributions. The procedure works the same way as in the NLO case which is explained in Sec. 4.2; it is important to take the limit $\eta \to 0$ before $\epsilon \to 0$. Some Hypergeometric functions can be expanded with the mathematica package HypExp [28], while others require some more work. See App. D.1 for details.

6.1 Renormalization

The full bare result can be split into a renormalization factor, Z, that contains all the divergences and a renormalized soft function, S_R, that only contains finite terms,

$$S_B(\mathbf{p}_\perp) = Z(\mu, \nu) \otimes_\perp S_R(\mathbf{p}_\perp, \mu, \nu). \quad (6.2)$$

We will write the renormalized soft function and renormalization factor as a power series in α_s,

$$S_R(\mathbf{p}_\perp, \mu, \nu) = \sum_{n=0}^{\infty} S_R^{(n)}(\mathbf{p}_\perp, \mu, \nu)\left(\frac{\alpha_s(\mu)}{4\pi}\right)^n, \quad Z(\mathbf{p}_\perp, \mu, \nu) = \sum_{n=0}^{\infty} Z^{(n)}(\mathbf{p}_\perp, \mu, \nu)\left(\frac{\alpha_s(\mu)}{4\pi}\right)^n. \quad (6.3)$$

To zeroth order we have $S_R^{(0)}(\mathbf{p}_\perp) = \delta^{(2)}(\mathbf{p}_\perp)$ and $Z^{(0)}(\mathbf{p}_\perp) = \mathbb{I}_p \equiv (2\pi)^2\delta^{(2)}(\mathbf{p}_\perp)$. Hence, an expansion of the bare function in Eq. (6.2) takes the form

$$S_B = \delta^{(2)}(\mathbf{p}_\perp) + \left(\frac{\alpha_s}{4\pi}\right)\left(S_R^{(1)} + \frac{1}{(2\pi)^2}Z^{(1)}\right) + \left(\frac{\alpha_s}{4\pi}\right)^2\left(S_R^{(2)} + Z^{(1)} \otimes_\perp S_R^{(1)} + \frac{1}{(2\pi)^2}Z^{(2)}\right) + \mathcal{O}(\alpha_s^3). \quad (6.4)$$

This can be matched up to the full expanded bare result in Eq. (6.1) and we get the renormalized NLO soft function coefficient

$$S_R^{(1)} = C_F w^2\left[-\frac{\pi^2\delta^{(2)}(\mathbf{p}_\perp)}{3} + 8\mathcal{L}_1 - 16\mathcal{L}_0\log\frac{\mu}{\nu}\right] + \mathcal{O}\left(\frac{\eta}{\epsilon^n}\right) + \mathcal{O}(\epsilon), \quad (6.5)$$

where $n \leq 3$. The terms that are proportional to η and ϵ are important since they produce finite terms in the $Z^{(1)} \otimes_\perp S^{(1)}$ term in Eq. (6.4) and are thus needed to extract $S_R^{(2)}$ and $Z^{(2)}$, but they play no further role since $\eta/\epsilon^n \to 0$ for all n and we will therefore not write them down. In addition, one needs to keep the $\mathcal{O}(\epsilon^3/\eta)$ terms in $Z^{(1)}$. The next coefficient is

$$\begin{aligned} S_R^{(2)} =& w^2\left\{C_F^2 w^2\left[-16\mathcal{L}_3 + 96\log\frac{\mu}{\nu}\mathcal{L}_2 - \left(\frac{8\pi^2}{3} + 128\log^2\frac{\mu}{\nu}\right)\mathcal{L}_1\right.\right. \\ &+ \left(64\zeta(3) + \frac{16\pi^2}{3}\log\frac{\mu}{\nu}\right)\mathcal{L}_0 + \left.\left(\frac{\pi^4}{18} + 64\zeta(3)\log\frac{\mu}{\nu}\right)\delta^{(2)}(\mathbf{p}_\perp)\right] \\ &+ 8C_F\beta_0\mathcal{L}_2 + \left[2\Gamma_1^q - 16C_F\beta_0\log\frac{\mu}{\nu}\right]\mathcal{L}_1 + \left[\frac{4\pi^2 C_F\beta_0}{3} - 4\Gamma_1^q\log\frac{\mu}{\nu}\right]\mathcal{L}_0 \\ &+ C_F\left[\frac{53\pi^4 C_A}{360} - \frac{(67C_A - 20T_F n_f)\pi^2}{18} + \frac{2428C_A - 656T_F n_f}{81}\right. \\ &\left.\left.+ \frac{2\beta_0\zeta(3)}{3} + \left(\frac{(1616C_A - 448T_F n_f)}{27} - 56\zeta(3)C_A\right)\log\frac{\mu}{\nu}\right]\delta^{(2)}(\mathbf{p}_\perp)\right\}, \end{aligned} \quad (6.6)$$

while the divergent terms are contained in

$$Z^{(1)} =16\pi^2 C_F w^2 \left[\frac{1}{\eta}\left(4\mathcal{L}_0 - \frac{2}{\epsilon}\delta^{(2)}(\mathbf{p}_\perp) + \mathcal{O}(\epsilon)\right) + \left(\frac{1}{\epsilon^2} + \frac{2}{\epsilon}\log\frac{\mu}{\nu}\right)\delta^{(2)}(\mathbf{p}_\perp)\right], \tag{6.7}$$

$$\begin{aligned} Z^{(2)} =& w^2\left\{32\pi^2 C_F^2 w^2\left[\frac{1}{\eta^2}\left(-32\mathcal{L}_1 - \frac{16}{\epsilon}\mathcal{L}_0 + \left(\frac{4}{\epsilon^2} - \frac{2\pi^2}{3}\right)\delta^{(2)}(\mathbf{p}_\perp)\right)\right.\right. \\ &+ \frac{1}{\eta}\left(4\mathcal{L}_2 + \left(\frac{8}{\epsilon} + 16\log\frac{\mu}{\nu}\right)\mathcal{L}_1 + \left(\frac{-2\pi^2}{3} + \frac{8}{\epsilon^2} + \frac{16}{\epsilon}\log\frac{\mu}{\nu}\right)\mathcal{L}_0\right. \\ &+ \left.\left(-\frac{4}{\epsilon^3} + \frac{\pi^2}{3\epsilon} + \frac{4\zeta(3)}{3} + \left(\frac{2\pi^2}{3} - \frac{8}{\epsilon^2}\right)\log\frac{\mu}{\nu}\right)\delta^{(2)}(\mathbf{p}_\perp)\right) \\ &+ \delta^{(2)}(\mathbf{p}_\perp)\left(\frac{1}{\epsilon^4} + \frac{4}{\epsilon^3}\log\frac{\mu}{\nu} + \frac{4}{\epsilon^2}\log^2\frac{\mu}{\nu}\right)\Bigg] + \frac{16\pi^2}{\eta}\left[4C_F\beta_0\mathcal{L}_1 + \Gamma_1^q\mathcal{L}_0\right. \\ &+ \left.C_F\left(\frac{-404C_A}{27} + \frac{112T_F n_f}{27} + \frac{\beta_0}{\epsilon^2} - \frac{\Gamma_1^q}{4C_F\epsilon} + 14C_A\zeta(3)\right)\delta^{(2)}(\mathbf{p}_\perp)\right] \\ &+ 16\pi^2\delta^{(2)}(\mathbf{p}_\perp)\left[-\frac{3C_F\beta_0}{4\epsilon^3} + \frac{C_F}{\epsilon^2}\left[\left(\frac{4n_f T_F}{3} - \frac{11C_A}{3}\right)\log\left(\frac{\mu}{\nu}\right) - \frac{\pi^2 C_A}{12} + \frac{67C_A}{36}\right.\right. \\ &- \left.\frac{5n_f T_F}{9}\right] + \frac{C_F}{\epsilon}\left(\left(-\frac{\pi^2 C_A}{3} + \frac{67C_A}{9} - \frac{20n_f T_F}{9}\right)\log\left(\frac{\mu}{\nu}\right) + \pi^2\left(\frac{n_f T_F}{18} - \frac{11C_A}{72}\right)\right. \\ &\left.\left.\left.\left. - \frac{7C_A\zeta(3)}{2} + \frac{101C_A}{27} - \frac{28n_f T_F}{27}\right)\right]\right\}. \end{aligned} \tag{6.8}$$

At this stage, we could set $w = 1$ in the renormalized result. However it is important to keep it in Z since it will play a role when deriving the ν anomalous dimension. The $\mathcal{L}_n$ factors are plus distributions which can be found in App. C.

6.2 Anomalous Dimensions

The fact that the bare soft function should not depend on the renormalization scale allows one to derive a RGE for the renormalized soft function. Demanding this of Eq. (6.2) gives

$$0 = \mu\frac{d}{d\mu}S_B(\mathbf{p}_\perp) = \left(\mu\frac{d}{d\mu}Z(\mu,\nu)\right)\otimes_\perp S_R(\mathbf{p}_\perp,\mu,\nu) + Z(\mu,\nu)\otimes_\perp\left(\mu\frac{d}{d\mu}S_R(\mathbf{p}_\perp,\mu,\nu)\right). \tag{6.9}$$

The RGE can then be obtained by just rearranging the above equation and an analogous argument holds for the parameter ν which results in a RRGE. We will write these as

$$\mu\frac{d}{d\mu}S_R(\mathbf{p}_\perp,\mu,\nu) = \gamma_{S_\mu}(\mu,\nu)\otimes_\perp S_R(\mathbf{p}_\perp,\mu,\nu), \tag{6.10}$$

$$\nu\frac{d}{d\nu}S_R(\mathbf{p}_\perp,\mu,\nu) = \gamma_{S_\nu}(\mu)\otimes_\perp S_R(\mathbf{p}_\perp,\mu,\nu), \tag{6.11}$$

where we have defined the two anomalous dimensions

$$\gamma_{S_\mu}(\mathbf{p}_\perp,\mu,\nu) \equiv -Z^{-1}(\mu,\nu)\otimes_\perp\left(\mu\frac{d}{d\mu}Z(\mathbf{p}_\perp,\mu,\nu)\right), \tag{6.12}$$

$$\gamma_{S_\nu}(\mathbf{p}_\perp,\mu) \equiv -Z^{-1}(\mu,\nu)\otimes_\perp\left(\nu\frac{d}{d\nu}Z(\mathbf{p}_\perp,\mu,\nu)\right). \tag{6.13}$$

The anomalous dimensions are however connected and we will eventually derive the structure of γ_{S_ν} from γ_{S_μ}.

With the results from Sec. 6.1 we can compute the anomalous dimensions. The expanded RGE takes the form

$$\begin{aligned}\gamma_{S_\mu} =& -\mu\frac{d}{d\mu}\left[Z^{(1)}\left(\frac{\alpha_s(\mu)}{4\pi}\right)\right] - \mu\frac{d}{d\mu}\left[Z^{(2)}\left(\frac{\alpha_s(\mu)}{4\pi}\right)^2\right] \\ &+ \left(\frac{\alpha_s(\mu)}{4\pi}\right) Z^{(1)} \otimes_\perp \mu\frac{d}{d\mu}\left[Z^{(1)}\left(\frac{\alpha_s(\mu)}{4\pi}\right)\right] + \mathcal{O}(\alpha_s^3).\end{aligned} \tag{6.14}$$

Because of the last term, one should remember to expand $Z^{(1)}$ to sufficient order. Here, one needs up to and including $\mathcal{O}(\epsilon^2/\eta)$. All the μ dependence sits in factors of $\mathcal{L}_n$, $\log(\mu/\nu)$ and $\alpha_s(\mu)$, which obeys Eq. (A.6). In the end, we arrive at the result[1]

$$\begin{aligned}\gamma_{S_\mu}(\mathbf{p}_\perp,\mu,\nu) =& \mathbb{I}_p\left\{4\left[\Gamma_0^q\left(\frac{\alpha_s(\mu)}{4\pi}\right) + \Gamma_1^q\left(\frac{\alpha_s(\mu)}{4\pi}\right)^2\right]\log\frac{\mu}{\nu}\right. \\ &\left. + \left(\frac{\alpha_s(\mu)}{4\pi}\right)^2 C_F\left[C_A\left(\frac{1616}{27} - \frac{22\pi^2}{9} - 56\zeta(3)\right) + T_F n_f\left(\frac{8\pi^2}{9} - \frac{448}{27}\right)\right]\right\}.\end{aligned} \tag{6.15}$$

The same can be done for γ_ν. One thing to remember is that the w book keeping parameter is ν dependent through Eq. (A.6), while all the other ν dependence is in $\log\frac{\mu}{\nu}$. The result is

$$\begin{aligned}\gamma_{S_\nu}(\mathbf{p}_\perp,\mu) =& 4(2\pi)^2\left\{\mathcal{L}_0\left[\Gamma_0^q\left(\frac{\alpha_s(\mu)}{4\pi}\right) + \Gamma_1^q\left(\frac{\alpha_s(\mu)}{4\pi}\right)^2\right] + 4\mathcal{L}_1 C_F\beta_0\left(\frac{\alpha_s(\mu)}{4\pi}\right)^2\right\} \\ &+ \mathbb{I}_p\left(\frac{\alpha_s(\mu)}{4\pi}\right)^2 C_F\left[C_A\left(56\zeta(3) - \frac{1616}{27}\right) + \frac{448 T_F n_f}{27}\right].\end{aligned} \tag{6.16}$$

6.3 Cross Checks

Given that the structures of the μ anomalous dimensions are known in our scheme, and that we can derive a relation between them, allows us to fully derive the structure of the soft and beam functions to all orders [29, 30]. This will be done by deriving a recursive relation for the soft function, and similarly for the beam functions in Sec. 7.2, which we will use to get the full structure up to NNLO. That this structure then matches our results from the actual computation will be a very strong cross check of our calculations. The only missing pieces will be the constants of the anomalous dimensions and the soft function, i.e. terms that are independent of $\mathbf{b}$, μ and ν.

6.3.1 Structure of γ_{S_ν}

First of all, we will derive γ_{S_ν} from the μ anomalous dimension. Because of the convolutions in momentum space, we will here go to position space where convolutions turn into simple products and plus distributions turn into ordinary logarithms, see Tab. C.1

[1] In all final results we set $w = 1$.

and C.2. Translation between the soft function in the fundamental and adjoint representation is straightforward and we will here express everything in full generality. We begin by writing the μ anomalous dimension as a power series in α_s, which in position space takes the Sudakov form[8]

$$\gamma^i_{S\mu}(\mu,\nu) = 4\Gamma^i_{\text{cusp}}[\alpha_s(\mu)]\log\frac{\mu}{\nu} + \gamma^i_S = \sum_{n=0}^{\infty}\left(4\Gamma^i_n\log\frac{\mu}{\nu} + \gamma^i_{Sn}\right)\left(\frac{\alpha_s(\mu)}{4\pi}\right)^{n+1}, \tag{6.17}$$

where the index i denotes the fundamental, $i = q$, or the adjoint representation, $i = g$. The cusp anomalous dimension is known up to three loops, while the non-cusp terms are something that we need to calculate. The fact that the cross section is independent of μ and ν and that derivatives commute,

$$\left[\frac{d}{d\mu}, \frac{d}{d\nu}\right] = 0, \tag{6.18}$$

gives us the relation [8]

$$\mu\frac{d}{d\mu}\gamma^i_{S/B_\nu} = \nu\frac{d}{d\nu}\gamma^i_{S/B_\mu} = -n\Gamma^i_{\text{cusp}}, \tag{6.19}$$

where $n = 2$ for the beam function and $n = 4$ for the soft function. We will use this to derive the structure of the ν anomalous dimension. First we note that γ_{S_ν} is ν independent and can thus be written as

$$\gamma^i_{S\nu}(\mathbf{b},\mu) \equiv \gamma^i_\nu(\mathbf{b},\mu) = \sum_{n=0}^{\infty}\gamma_\nu^{i\,(n)}(\mathbf{b},\mu)\left(\frac{\alpha_s(\mu)}{4\pi}\right)^{n+1}. \tag{6.20}$$

If we then take the μ derivative of this we get

$$\begin{aligned}
\mu\frac{d}{d\mu}\gamma^i_\nu =& \sum_{n=0}^{\infty}\left[\mu\frac{d\gamma_\nu^{i\,(n)}}{d\mu}\left(\frac{\alpha_s}{4\pi}\right)^{n+1} - 2\gamma_\nu^{i\,(n)}\frac{(n+1)}{4\pi}\left(\frac{\alpha_s}{4\pi}\right)^{n}\mu\frac{d\alpha_s}{d\mu}\right] \\
=& \sum_{n=0}^{\infty}\left[\mu\frac{d\gamma_\nu^{i\,(n)}}{d\mu} - 2(n+1)\gamma_\nu^{i\,(n)}\sum_{m=0}^{\infty}\beta_m\left(\frac{\alpha_s}{4\pi}\right)^{m+1}\right]\left(\frac{\alpha_s}{4\pi}\right)^{n+1} \\
=& \mu\frac{d\gamma_\nu^{i\,(0)}}{d\mu}\left(\frac{\alpha_s}{4\pi}\right) + \sum_{n=1}^{\infty}\left[\mu\frac{d\gamma_\nu^{i\,(n)}}{d\mu} - 2\sum_{m=0}^{n-1}(m+1)\gamma_\nu^{i\,(m)}\beta_{n-m-1}\right]\left(\frac{\alpha_s}{4\pi}\right)^{n+1}.
\end{aligned} \tag{6.21}$$

By comparing this to Eq. (6.19) and matching up the α_s coefficients we get a recursive relation for the $\gamma_\nu^{i\,(n)}$ functions which we can integrate and obtain

$$\gamma_\nu^{i\,(0)}(\mathbf{b},\mu) = -2\Gamma^i_0\log\frac{\mu^2}{\mu_S^2} + \gamma_\nu^{i\,(0)}(\mathbf{b},\mu_S), \tag{6.22}$$

$$\begin{aligned}
\gamma_\nu^{i\,(n)}(\mathbf{b},\mu) =& -2\Gamma^i_n\log\frac{\mu^2}{\mu_S^2} \\
&+ 2\sum_{m=0}^{n-1}(m+1)\beta_{n-m-1}\int_{\mu_S}^{\mu}d\log\mu'\gamma_\nu^{i\,(m)}(\mu') + \gamma_\nu^{i\,(n)}(\mathbf{b},\mu_S), \quad n \geq 1.
\end{aligned} \tag{6.23}$$

The $\gamma_\nu^{i\,(n)}(\mathbf{b},\mu_S)$ are the boundary conditions of the integration. Guided by the results from the calculation of the soft function and the Fourier transform of the plus distributions, we set the canonical boundary condition $\mu_S^2 = 4\mathbf{b}^{-2}e^{-2\gamma_E}$. This will ensure that these terms are $\mathbf{b}$ independent since they are dimensionless; hence they are the pure numbers that need to be calculated explicitly and we denote them with a new notation

$$\gamma_\nu^{i\,(n)}(\mathbf{b},\mu_S)\Big|_{\mu_S=4\mathbf{b}^{-2}e^{-2\gamma_E}} \equiv \gamma_{\nu n}^i. \tag{6.24}$$

For later convenience, we also define the logarithm

$$L_b \equiv \log\left(\frac{\mathbf{b}^2\mu^2 e^{2\gamma_E}}{4}\right). \tag{6.25}$$

6.3.2 Structure of the soft function

Since we now know the structure of both the μ and ν anomalous dimensions we can derive a recursive relation for the renormalized soft function as well. From here on we will suppress the R notation for renormalized; moreover, we introduce an index i for quark, $i = q$, or gluon, $i = g$, soft function. In position space we write the soft function as

$$S^i(\mathbf{b},\mu,\nu) = \frac{1}{(2\pi)^2}\sum_{n=0}^{\infty} S^{i(n)}(\mathbf{b},\mu,\nu)\left(\frac{\alpha_s}{4\pi}\right)^n. \tag{6.26}$$

The μ derivative of this leads to

$$\mu\frac{dS^i}{d\mu} = \frac{1}{(2\pi)^2}\mu\frac{dS^{i(0)}}{d\mu} + \frac{1}{(2\pi)^2}\sum_{n=1}^{\infty}\left[\mu\frac{dS^{i(n)}}{d\mu} - 2\sum_{m=0}^{n-1} m\beta_{n-m-1}S^{i(m)}\right]\left(\frac{\alpha_s}{4\pi}\right)^n. \tag{6.27}$$

Which by the RGE should be equal to

$$\mu\frac{dS^i}{d\mu} = \gamma_{S_\mu}^i S^i = \frac{1}{(2\pi)^2}\sum_{n=1}^{\infty}\sum_{m=0}^{n-1}\left(4\Gamma_m^i\log\frac{\mu}{\nu} + \gamma_{Sm}^i\right)S^{i(n-m-1)}\left(\frac{\alpha_s}{4\pi}\right)^n. \tag{6.28}$$

Integrating this leads to the first recursive relation for the soft function. For $n \geq 1$ the soft coefficients obey

$$\begin{aligned} S^{i(n)}(\mathbf{b},\mu,\nu) = \sum_{m=0}^{n-1}\Bigg[&(2m\beta_{n-m-1} + \gamma_{Sn-m-1}^i)\int_{\mu_S}^{\mu}\frac{d\mu'}{\mu'}S^{i(m)}(\mathbf{b},\mu',\nu) \\ &+4\Gamma_{n-m-1}^i\int_{\mu_S}^{\mu}\frac{d\mu'}{\mu'}\log\frac{\mu'}{\nu}S^{i(m)}(\mathbf{b},\mu',\nu)\Bigg] + S^{i(n)}(\mathbf{b},\mu_S,\nu). \end{aligned} \tag{6.29}$$

Similar manipulation of the RRGE gives a second recursive relation

$$S^{i(n)}(\mathbf{b},\mu,\nu) = \sum_{m=0}^{n-1}\gamma_\nu^{i\,(n-m-1)}(\mathbf{b},\mu)\int_{\nu_S}^{\nu}\frac{d\nu'}{\nu'}S^{i(m)}(\mathbf{b},\mu,\nu') + S^{i(n)}(\mathbf{b},\nu_S,\mu). \tag{6.30}$$

The complete solution for the soft function is obtained by substituting the boundary term in Eq. (6.29) for Eq. (6.30). We fix the final boundary term with the canonical choice

$\mu_S = \nu_S = 4\mathbf{b}^{-2}e^{-2\gamma_E}$ which means that they are pure numbers. This results in the full solution of the soft function for $n \geq 1$:

$$S^{i(n)}(\mathbf{b},\mu,\nu) = \sum_{m=0}^{n-1}\Bigg\{\left[2m\beta_{n-m-1}+\gamma^i_{Sn-m-1}\right]\int_{\mu_S}^{\mu}\frac{d\mu'}{\mu'}S^{i(m)}(\mathbf{b},\mu',\nu)$$
$$+4\Gamma^i_{n-m-1}\int_{\mu_S}^{\mu}\frac{d\mu'}{\mu'}\log\frac{\mu'}{\nu}S^{i(m)}(\mathbf{b},\mu',\nu)+\gamma^i_{\nu n-m-1}\int_{\nu_S}^{\nu}\frac{d\nu'}{\nu'}S^{i(m)}(\mathbf{b},\mu_S,\nu')\Bigg\}+S^i_n, \quad (6.31)$$

where S^i_n is a pure number.

6.3.3 Results in position space

With the recursive relation for the γ^i_ν in Eq. (6.22), we get to $\mathcal{O}(\alpha_s^2)$:

$$\gamma^i_\nu\left[L_b,\alpha_s(\mu)\right] = \left(-2\Gamma^i_0 L_b+\gamma^i_{\nu 0}\right)\left(\frac{\alpha_s(\mu)}{4\pi}\right)+\left(-\beta_0\Gamma^i_0 L_b^2-2\Gamma^i_1 L_b+\gamma^i_{\nu 1}\right)\left(\frac{\alpha_s(\mu)}{4\pi}\right)^2. \quad (6.32)$$

With this and the recursive relation in Eq. (6.31), one can also derive the structure of the NNLO renormalized soft function. Both the soft function and γ_ν are in perfect agreement to the results from our explicit calculations in Eq. (6.5), (6.6) and (6.16), once transformed to momentum space. Here, we present the soft function in position space where we write it as

$$\begin{aligned}S^i\left[L_b,\mu/\nu,\alpha_s(\mu)\right] =& \frac{1}{(2\pi)^2}\Bigg\{1+\left(\frac{\alpha_s(\mu)}{4\pi}\right)\left[S^i_1+2\Gamma^i_0\log\frac{\mu}{\nu}L_b-\frac{\Gamma^i_0}{2}L_b^2\right]\\ &+\left(\frac{\alpha_s(\mu)}{4\pi}\right)^2\Bigg[S^i_2-\gamma^i_{\nu 1}\log\frac{\mu}{\nu}\\ &+\left(\frac{\gamma^i_{\nu 1}}{2}+\beta_0 S^i_1+\frac{\gamma^i_{S1}}{2}+2(S^i_1\Gamma^i_0+\Gamma^i_1)\log\frac{\mu}{\nu}\right)L_b\\ &+\left(-\frac{S^i_1\Gamma^i_0}{2}-\frac{\Gamma^i_1}{2}+\beta_0\Gamma^i_0\log\frac{\mu}{\nu}+2\Gamma^i_0\log^2\frac{\mu}{\nu}\right)L_b^2\\ &+\left(-\frac{\beta_1\Gamma^i_0}{3}-{\Gamma^i_0}^2\log\frac{\mu}{\nu}\right)L_b^3+\frac{{\Gamma^i_0}^2}{8}L_b^4\Bigg]\Bigg\}. \end{aligned} \quad (6.33)$$

The cusp anomalous dimension can be found in App. A while the new terms that we calculated in this thesis are the non-cusp terms which are defined by Eq. (6.17) and (6.32), as well as the S^i_n constant terms. Matching onto the results from our momentum space

NNLO calculation, in Eq. (6.5),(6.6), (6.15) and (6.16), gives

$$\begin{aligned}
\gamma^i_{S0} =& \gamma^i_{\nu 0} = 0, \\
\gamma^i_{S1} =& \mathcal{C}^i \left[C_A \left(\frac{1616}{27} - \frac{22\pi^2}{9} - 56\zeta(3) \right) + T_F n_f \left(\frac{8\pi^2}{9} - \frac{448}{27} \right) \right], \qquad (6.34) \\
\gamma^i_{\nu 1} =& \mathcal{C}^i \left[C_A \left(56\zeta(3) - \frac{1616}{27} \right) + \frac{448 T_F n_f}{27} \right], \qquad (6.35) \\
S^i_1 =& -\frac{\mathcal{C}^i \pi^2}{3}, \qquad (6.36) \\
S^i_2 =& \frac{{\mathcal{C}^i}^2 \pi^4}{18} + \mathcal{C}^i \left\{ \frac{[C_A(97120 - 12060\pi^2 + 477\pi^4 - 55440\zeta(3)]}{3240} \right. \\
& \left. + \frac{2 T_F n_f}{81} \left[-328 + 45\pi^2 + 252\zeta(3) \right] \right\}. \qquad (6.37)
\end{aligned}$$

The color factors are here expressed in a more general form with the index i. For a soft function in the fundamental representation we can identify $\mathcal{C}^q = C_F$ and for the adjoint representation we have $\mathcal{C}^g = C_A$.

Chapter 7

Beam Functions and Higgs Production

One important example where SCET has been successfully applied to resum large logarithms is Higgs production at low $\mathbf{p}_\perp$ [8, 11, 31, 10] and the differential cross section $d\sigma/d\mathbf{p}_T^2$ has been computed up to NNLL+NNLO in two different frameworks [10, 11]. The work in Ref. [10] has been done in the framework layed out in Ref. [31, 32], which we will call the BNW[1] formalism; While Ref. [11] uses the same framework as we have been using in this thesis [8, 9], which we will call the CJNR[2] formalism.

In contrast to the CJNR formalism, BNW's resummation of rapidity logarithms is not based on a renormalization group. The method of resumming rapidity logarithms in BNW essentially fixes the renormalization scale ν to its natural scale. This can be compared to CJNR where one is free to choose ν and this provides the possibility to perform an extended set of scale variations to probe the uncertainties related to the resummation.

The beam functions also goes by the name Transverse Momentum Dependent Parton Distribution Functions (TMDPDF) and have been calculated to NNLO in the BNW formalism [12, 13]. In this chapter, we will see how the two formalisms are related and we will translate the beam functions from the BNW scheme to the CJNR scheme. Similar to the case of the soft function, we can derive the structure of the beam functions to NNLO straight from its anomalous dimensions. The hard function in the factorization theorem does not differ between the two formalisms and thus the product of beam and soft functions must agree in the end. Hence, we can then find all the missing constants in our beam functions by comparing the full combined result of our beam and soft functions to the beam functions in Ref. [12].

With the beam and soft functions to NNLO, all necessary ingredients are known to compute the cross section to NNLL′+NNLO. The prime denotes that in addition to the NNLL resummation one also includes all the $\mathcal{O}(\alpha_s^2)$ terms of the hard, soft and beam functions appearing in the factorization theorem. This contribution is formally part of the N^{3}LL resummation but this prime way of counting is in many ways more systematic [33]. The counting prescription and necessary ingredients to perform the full resummation at each order can be read off Tab. 7.1.

[1] Thomas Becher, Matthias Neubert and Daniel Wilhelm.
[2] Jui-yu Chiu, Ambar Jain, Duff Neill and Ira Z. Rothstein

Resummation	H, B, S	Γ_{cusp}	γ_H, γ_B, γ_S, γ_ν	$\beta[\alpha_s]$
LL	Tree-level	1-loop	-	1-loop
NLL	Tree-level	2-loop	1-loop	2-loop
NLL′	1-loop	2-loop	1-loop	2-loop
NNLL	1-loop	3-loop	2-loop	3-loop
NNLL′	2-loop	3-loop	2-loop	3-loop
N^{3}LL	2-loop	4-loop	3-loop	4-loop

Table 7.1: Necessary ingredients to aquire N^{n}LL and N^{n}LL′ resummation accuracy. With the results from this thesis, one can now perform NNLL′ resummation in this formalism which we are working in.

7.1 Cross Section

The derivation of the $\mathbf{p}_\perp^2$ differential cross section for Higgs production in SCET can be found in Ref. [8, 10]. Here we follow a similar path and consider Higgs production through gluon fusion. The factorization of $pp \to XH$ is done essentially in the same way as in Chap. 3 but with gluon beam functions instead of quark beam functions and the color-singlet L corresponds to the Higgs. Here we simply present the final form of the differential cross section:

$$\frac{d\sigma}{d\mathbf{p}_\perp^2 dy} = \sigma_0(\mu) C_t^2(m_t^2,\mu)|C_s(-m_h^2,\mu)|^2(2\pi)^6 \int \frac{d^2b}{(2\pi)^2} e^{-i\mathbf{b}\cdot\mathbf{p}_\perp} \times 2B_g^{\mu\nu}\left(\frac{m_h}{\sqrt{s}}e^{y},\mathbf{b}\right) B_{g_{\mu\nu}}\left(\frac{m_h}{\sqrt{s}}e^{-y},\mathbf{b}\right) S(\mathbf{b}). \quad (7.1)$$

All Wilson coefficients and constants that are relevant to NNLL′ can be found in App. E. The beam functions are matched onto standard non-perturbative PDFs like[8, 34]

$$B_g^{\mu\nu}(z,\mathbf{b},\mu,\nu,\omega) = \sum_{i=g,q,\bar{q}} \left[\frac{g_\perp^{\mu\nu}}{2}\mathcal{I}_{gi}(\mu,\nu/\omega,\mathbf{b}) + \left(\frac{g^{\mu\nu}}{2} - \frac{b^\mu b^\nu}{b^2}\right)\mathcal{J}_{gi}(\mu,\nu/\omega,\mathbf{b})\right] \otimes_z f_i(\mu,z), \quad (7.2)$$

where we have defined the convolution for the light-cone component $z_\pm = \frac{m_h}{\sqrt{s}}e^{\pm y}$ as

$$f \otimes_z g(z) \equiv \int_z^1 \frac{dw}{w} f(w) g\left(\frac{z}{w}\right). \quad (7.3)$$

The two different tensor structures in Eq. (7.2) correspond to polarization independent, $\mathcal{I}_{gi}$, and dependent, $\mathcal{J}_{gi}$, parts. The large momentum component that enters the hard process is denoted by ω.

7.1.1 RG evolution

Since the resummation of the rapidity logarithms has already been performed in Ref. [10], we need to do that as well before comparing our two formalisms. Our rapidity regulator gives rise to a RRGE that enables us to sum up all rapidity logarithms by evolving the beam and soft function from their natural scale to a common arbitrary point in the 2-dimensional RG-space, see Fig. 7.1. The natural scale for each function can be identified

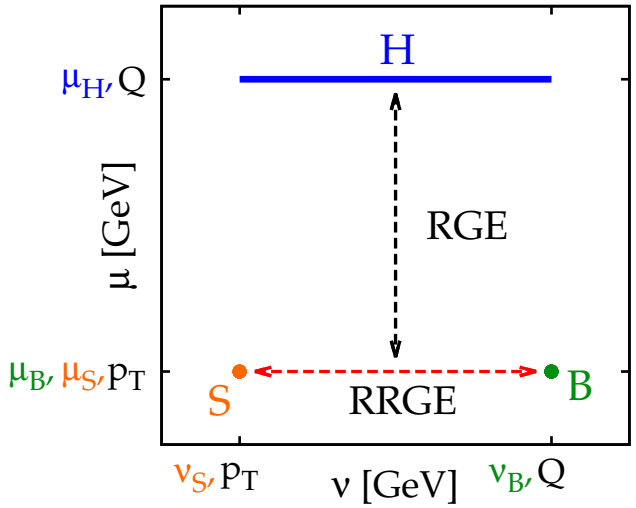

Figure 7.1: Evolution of the hard, soft and beam functions in the μ, ν-space through RGE and RRGE. Note that the hard function is ν independent.

by looking at the arguments of the logarithms in the fixed order result; thus we can fix the canonical values for the soft scales μ_S and ν_S from our previous calculations. The beam function will be derived in Sec. 7.2 and, using this result, we find the natural scales

$$\nu_S \sim \mu_S \sim \mu_B \sim |\mathbf{p}_\perp| \sim 1/|\mathbf{b}|, \tag{7.4}$$

$$\nu_B \sim \omega^\pm \sim Q, \tag{7.5}$$

$$\mu_H \sim Q \sim m_h.$$

Solving the RGE/RRGE is relatively straightforward and results in evolution functions. Here we only present the rapidity evolution since it is the only one we need for our comparison. The RRGE for the soft and beam functions are in position space

$$\nu \frac{d}{d\nu} S^g(\mathbf{b}, \mu, \nu) = \gamma_\nu^g(\mu) S^g(\mathbf{b}, \mu, \nu), \tag{7.6}$$

$$\nu \frac{d}{d\nu} B_g^{\rho\sigma}(\mathbf{b}, \mu, \nu) = -\frac{1}{2} \gamma_\nu^g(\mu) B_g^{\rho\sigma}(\mathbf{b}, \mu, \nu), \tag{7.7}$$

with the solutions

$$S^g(\mathbf{b}, \mu, \nu) = \exp\left(\gamma_\nu^g(\mathbf{b}, \mu) \log \frac{\nu}{\nu_S}\right) S^g(\mathbf{b}, \mu, \nu_S), \tag{7.8}$$

$$B_g^{\rho\sigma}(\mathbf{b}, \mu, \nu) = \exp\left(-\frac{1}{2}\gamma_\nu^g(\mathbf{b}, \mu) \log \frac{\nu}{\nu_B}\right) B_g^{\rho\sigma}(\mathbf{b}, \mu, \nu_B), \tag{7.9}$$

where ν_B is the large momentum in each collinear direction, $\nu_B^2 = \omega^+\omega^- = Q^2$. If we combine the evolution factors of the soft and two beam functions, we will get the full rapidity resummation which gives a factor of

$$\exp\left[\gamma_\nu^g(\mathbf{b}, \mu)\left(\log \frac{\nu}{\nu_S} + \log\sqrt{\frac{\nu_B}{\nu}} + \log\sqrt{\frac{\nu_B}{\nu}}\right)\right] = \left(\frac{\nu_B^2}{\nu_S^2}\right)^{\frac{1}{2}\gamma_\nu^g(\mathbf{b},\mu)}, \tag{7.10}$$

to the cross section. Setting $\nu_S^2 = 4e^{-2\gamma_E}/\mathbf{b}^2$ and $\nu_B^2 = m_h^2$ recovers the resummation in the BNW framework[3].

After the resummation of rapidity logarithms, we end up with the renormalized cross section that looks like

$$\begin{aligned}\frac{d\sigma}{d\mathbf{p}_\perp^2 dy} = \sigma_0(\mu) C_t^2(m_t^2,\mu)|C_s(-m_h^2,\mu)|^2(2\pi)^6 \int \frac{d^2b}{(2\pi)^2} e^{-i\mathbf{b}\cdot\mathbf{p}_\perp} \left(\frac{\nu_B^2}{\nu_S^2}\right)^{\frac{1}{2}\gamma_\nu^g(\mathbf{b},\mu)} S(\mathbf{b},\mu) \\ \times \sum_{i,j=g,q,\bar{q}} \{[\mathcal{I}_{gi}(\mathbf{b},\mu)\otimes_z f_i(z_+,\mu)]\,[\mathcal{I}_{gj}(\mathbf{b},\mu)\otimes_z f_j(z_-,\mu)] \\ + [\mathcal{J}_{gi}(\mathbf{b},\mu)\otimes_z f_i(z_+,\mu)]\,[\mathcal{J}_{gj}(\mathbf{b},\mu)\otimes_z f_j(z_-,\mu)]\}\,. \quad (7.11)\end{aligned}$$

This equation should be compared to Eq. 12 in Ref. [10]. Since the hard function is the same in both formalisms we can ignore it and only look at the beam functions combined with the soft function. By comparing them we obtain the relation

$$(2\pi)^6 \left(\frac{\nu_B^2}{\nu_S^2}\right)^{\frac{1}{2}\gamma_\nu^g} S \sum_{i,j=g,q,\bar{q}} [\mathcal{I}_{gi}\mathcal{I}_{gj} + \mathcal{J}_{gi}\mathcal{J}_{gj}] = \left(\frac{x_T^2 m_H^2 e^{2\gamma_E}}{4}\right)^{-F_{gg}} \sum_{i,j=g,q,\bar{q}} \left[I_{g/i}I_{g/j} + I'_{g/i}I'_{g/j}\right]. \quad (7.12)$$

We have expressed the right hand side in the notation of Ref. [10]; however, note that $x_T = \mathbf{b}$. The factor of $(2\pi)^6$ comes from different normalization conventions and the details about the matching coefficients $I_{g/i}$, which have been computed to NNLO, can be found in Ref. [12]. The $I'_{g/i}$ have been computed to NLO and are presented in Ref. [10]. Since the μ dependence is the same for both formalisms we can obtain our μ-anomalous dimension for the beam functions by taking the μ derivative of Eq. (7.12).

Quark beam function

Although the quark beam function is not required for gluon fusion we include it for completeness. The derivation of the relation corresponding to Eq. (7.12) look the same; however, the unpolarized quark beam function is a Lorentz scalar and thus does not have a tensor structure as the gluon one. Moreover, the flavor structure is more complicated because of flavor mixing. Here, we write the matching onto PDFs as

$$B_q(z,\mathbf{b},\mu,\nu/\omega) = \sum_{i=g,q,\bar{q}} \mathcal{I}_{qi}(\mu,\nu/\omega,\mathbf{b})\otimes_z f_i(z,\mu). \quad (7.13)$$

Then the relation to the matching kernels in Ref. [12] is

$$(2\pi)^6 \left(\frac{\nu_B^2}{\nu_S^2}\right)^{\frac{1}{2}\gamma_\nu^q} S \sum_{i,j=g,q,\bar{q}} \mathcal{I}_{qi}\mathcal{I}_{\bar{q}j} = \left(\frac{x_T^2 m_H^2}{b_0^2}\right)^{-F_{q\bar{q}}} \sum_{i,j=g,q,\bar{q}} I_{q/i}^{(n)} I_{\bar{q}/j}^{(n)}. \quad (7.14)$$

Note that the sum over i,j is over gluons as well as all quark flavors, i.e. there are matching coefficients for quark flavor mixing.

[3] See Eq. 6 in Ref. [10]. The rapidity logarithms are contained in $\left(x_T^2 m_H^2 e^{2\gamma_E}/4\right)^{-F_{gg}(x_T^2,\mu)}$ and indeed we find the relation $-F_{gg} = \frac{1}{2}\gamma_\nu^g$.

7.2 Structure of the Beam Functions

Before determining the constant pieces of the beam functions we can derive their structure from the anomalous dimension similar to the soft function case in Sec. 6.3.2. In the gluon beam function, the $\mathcal{I}_{gi}$ corresponds to the unpolarized part while the traceless $\mathcal{J}_{gi}$ is the polarized part. The derivation of the structure of the matching coefficients is independent of the polarization, and whether it is a quark or beam function, so we will only show the formulas for a general $\mathcal{I}_{ij}$, but the same formulas are valid for $\mathcal{J}_{gj}$.

We first derive a recursive relation for the matching coefficients which can be written as a series in α_s,

$$\mathcal{I}_{ij} = \frac{1}{(2\pi)^2} \sum_{n=0}^{\infty} {\mathcal{I}_{ij}}^{(n)} \left(\frac{\alpha_s}{4\pi}\right)^n. \tag{7.15}$$

The calculation is similar to the soft function so we will not write it down in great detail. The starting point is the RGE and RRGE,

$$\mu \frac{d}{d\mu} B_i = \gamma^i_{B\mu} B_i, \tag{7.16}$$

$$\nu \frac{d}{d\nu} B_i = -\frac{1}{2} \gamma^i_{\nu} B_i. \tag{7.17}$$

However, an additional complication is that the PDFs, $f_i(z,\mu)$, in Eq. (7.2) and (7.13) depends on μ through the equation [30, 29]

$$\frac{d}{d\log\mu} f_i(z,\mu) = 2 \sum_j P_{ij}[\alpha_s(\mu)] \otimes_z f_j(z,\mu), \tag{7.18}$$

where the DGLAP splitting functions, P_{ij} can be expanded like

$$P_{ij}[z,\alpha_s(z)] = \sum_{n=0}^{\infty} 2^{n+1} P^n_{ij}(z) \left(\frac{\alpha_s}{4\pi}\right)^{n+1}, \tag{7.19}$$

and all the necessary P^n_{ij} functions can be found in Ref. [30]. This results in the following RGE and RRGE

$$\frac{d\mathcal{I}_{ij}}{d\log\mu} = \sum_k \mathcal{I}_{ik} \otimes_z \left[\delta(1-z)\delta_{kj}\gamma^i_{B\mu} - 2P_{kj}[\alpha_s(\mu)]\right], \tag{7.20}$$

$$\frac{d\mathcal{I}_{ij}}{d\log\nu} = -\frac{1}{2}\gamma^i_{\nu}\mathcal{I}_{ij}. \tag{7.21}$$

With the anomalous dimensions [8],

$$\gamma^i_{B\mu}(\mu,\nu) = \sum_{n=0}^{\infty} \left[2\Gamma^i_n \log\frac{\nu}{\omega} + \gamma^i_{Bn}\right] \left(\frac{\alpha_s}{4\pi}\right)^{n+1}, \tag{7.22}$$

$$\gamma^i_{B\nu}(\mathbf{b},\mu) = -\frac{1}{2}\gamma^i_{\nu}(\mathbf{b},\mu) = -\frac{1}{2}\sum_{n=0}^{\infty} {\gamma^i_{\nu}}^{(n)}(\mathbf{b},\mu) \left(\frac{\alpha_s}{4\pi}\right)^{n+1}. \tag{7.23}$$

The last relation comes from the fact that the total cross section and the hard function does not depend on ν. As before, the procedure works as follows: insert all expansion

series and match up the coefficients of α_s in the RGE and RRGE; integrate them; and finally substitute the boundary term in the RGE solution with the RRGE solution. In the end, one ends up at a recursive relation for $n \geq 1$:

$$\begin{aligned}\mathcal{I}_{ij}^{(n)}(\mathbf{b},\mu,\nu) = \sum_{m=0}^{n-1}\Bigg[&\left(2\Gamma^i_{n-m-1}\log\frac{\nu}{\omega}+\gamma^i_{B\,n-m-1}+2m\beta_{n-m-1}\right)\int_{\mu_B}^{\mu}\frac{d\mu'}{\mu'}\mathcal{I}_{ij}^{(m)}(b,\mu',\nu)\\ &-2\sum_{\ell}2^{n-m}P_{\ell j}^{n-m-1}\otimes_z\int_{\mu_B}^{\mu}\frac{d\mu'}{\mu'}\mathcal{I}_{i\ell}^{(m)}(\mu',\nu)\\ &-\frac{1}{2}\gamma^i_{\nu\,n-m-1}\int_{\nu_B}^{\nu}\frac{d\nu'}{\nu'}\mathcal{I}_{ij}^{(m)}(b,\mu_B,\nu')\Bigg]+I_{ij}^{(n)}(z). \quad (7.24)\end{aligned}$$

We have, again, chosen the canonical scales $\mu_B = 4\mathbf{b}^{-2}e^{-2\gamma_E}$ and $\nu_B = \omega$ which makes the $I_{ij}^{(n)}(z)$ functions dimensionless.

7.3 Results in Position Space

Using the recursive relation in Eq. (7.24) we can compute the structure of the beam functions up to arbitrary constants at each order. The zeroth order is easy to obtain

$$\mathcal{I}_{ij}^{(0)}(z) = \delta_{ij}\delta(1-z), \quad (7.25)$$

$$\mathcal{J}_{gi}^{(0)}(z) = 0, \quad (7.26)$$

with which we get

$$\mathcal{I}_{ij}^{(1)}(L_b,z) = \left[(\Gamma_0^i\log\frac{\nu}{\omega}+\frac{1}{2}\gamma^i_{B0})\delta_{ij}\delta(1-z)-2P_{ij}^0\right]L_b + I_{ij}^{(1)}(z), \quad (7.27)$$

$$\mathcal{J}_{gi}^{(1)}(z) = J_{gi}^{(1)}(z). \quad (7.28)$$

and

$$\begin{aligned}\mathcal{I}_{ij}^{(2)}(L_b,\nu/\omega,z) = &\Bigg\{\left[(2\Gamma_0^i\log\frac{\nu}{\omega}+\gamma^i_{B0})^2+4\Gamma_0^i\beta_0\log\frac{\nu}{\omega}+2\beta_0\gamma^i_{B0}\right]\frac{\delta_{ij}\delta(1-z)}{8}\\ &-(2\Gamma_0^i\log\frac{\nu}{\omega}+\gamma^i_{B0}+\beta_0)P_{ij}^0(z)+2\sum_{k=g,q,\bar{q}}P_{kj}^0\otimes_z P_{ik}^0(z)\Bigg\}L_b^2\\ &\Bigg\{\left[(\Gamma_1^i\log\frac{\nu}{\omega}+\frac{1}{2}\gamma^i_{B1})\delta_{ij}\delta(1-z)-4P_{ij}^1(z)\right]\\ &+\left[\Gamma_0^i\log\frac{\nu}{\omega}+\frac{1}{2}\gamma^i_{B0}+\beta_0\right]I_{ij}^{(1)}(z)-2\sum_{k=g,q,\bar{q}}P_{kj}^0\otimes_z I_{ik}^{(1)}(z)\Bigg\}L_b\\ &-\frac{1}{2}\gamma^i_{\nu1}\delta_{ij}\delta(1-z)\log\frac{\nu}{\omega}+I_{ij}^{(2)}(z), \quad (7.29)\end{aligned}$$

$$\mathcal{J}_{gi}^{(2)}(L_b,\nu/\omega,z) = \left[\left(\Gamma_0^g\log\frac{\nu}{\omega}+\frac{1}{2}\gamma^g_{B0}+\beta_0\right)J_{gi}^{(1)}(z)-2\sum_{j=g,q,\bar{q}}P_{ji}^0\otimes_z J_{gj}^{(1)}(z)\right]L_b+J_{gj}^{(2)}(z). \quad (7.30)$$

All the $P_{ij}^n(z)$ functions can be found in Ref. [30].

The μ dependence of the beam functions is known up to two loops in the BNW scheme and hence we can obtain γ_B by taking the derivative of Eq. (7.12) and (7.14) and we find the relation

$$\gamma_B^i = -2\gamma^i - \frac{1}{2}\gamma_S^i, \tag{7.31}$$

where γ^i can be found in Ref. [12]. This results in

$$\begin{aligned}
\gamma_{B0}^g =& 2\beta_0, \\
\gamma_{B0}^q =& 6C_F, \\
\gamma_{B1}^g =& -\frac{32}{3}C_A T_F n_f - 8C_F T_F n_f + \frac{8}{27}C_A^2\left(81\zeta(3) - 274\right), \\
\gamma_{B1}^q =& -\frac{1}{9}C_F\left[C_A\left(216\zeta(3) - 51 - 44\pi^2\right)\right. \\
&\left. + 9C_F\left(-48\zeta(3) - 3 + 4\pi^2\right) + 4\left(3 + 4\pi^2\right)n_f T_F\right].
\end{aligned} \tag{7.32}$$

When fixing the beam function constants, we can choose $\mu^2 = 1/\mathbf{b}^2$ which eliminates all the logarithms and the matching becomes straightforward to do. We obtain the constant pieces

$$\begin{aligned}
I_{q'q}^{(1)}(z) =& I_{\bar{q}q}^{(1)}(z) = 0, \\
I_{gi}^{(1)}(z) =& 2C_F z(\delta_{qi} + \delta_{\bar{q}i}), \\
I_{qi}^{(1)}(z) =& 2C_F(1-z)\delta_{qi} + 2T_F z(2-z)\delta_{gi}, \\
I_{q'q}^{(2)}(z) =& I_{q'/q}^{(2)}(z,0), \\
I_{\bar{q}q}^{(2)}(z) =& I_{\bar{q}/q}^{(2)}(z,0), \\
I_{gi}^{(2)}(z) =& \frac{1}{2}\delta_{gi}\delta(1-z)\left[\left(\frac{C_A\pi^2}{6}\right)^2 - S_2^g\right] + \delta_{qi}\frac{C_F C_A \pi^2}{3}z + I_{g/i}^{(2)}(z,0), \\
I_{qi}^{(2)}(z) =& \frac{1}{2}\delta_{qi}\delta(1-z)\left[\left(\frac{C_F\pi^2}{6}\right)^2 - S_2^q\right] - \frac{C_F^2\pi^2}{3}\delta_{qi}(1-z) \\
&+ \frac{C_F T_F}{3}\delta_{gi}z(2-z) + I_{q/i}^{(2)}(z,0), \\
J_{gi}^{(1)}(z) =& 4\frac{1-z}{z}\left[C_A\delta_{gi} + C_F\left(\delta_{qi} + \delta_{\bar{q}i}\right)\right].
\end{aligned} \tag{7.33}$$

The $I_{g/i}^{(2)}$ functions can be found in Sec. 4 of Ref. [12].

The $J_{gi}^{(2)}$ matching kernels have not been calculated so we cannot extract $J_{gi}^{(2)}$. This does not matter though since $\mathcal{J}_{gi}$ starts at $\mathcal{O}(\alpha_s)$, in contrast to $\mathcal{I}_{gi}$, and they appear essentially as a square in the cross section. Thus, $J_{gi}^{(2)}$ is not needed for the NNLL′+NNLO cross section, i.e. the order we are interested in.

Chapter 8

Conclusion

This thesis concerns the transverse momentum distribution for the process $pp \to XL$, in the region $\mathbf{p}_\perp^2 \ll Q^2$. Using an effective field theory, SCET, to separate the relevant degrees of freedom in different momentum regions, we reviewed the factorization theorem for the cross section. This resulted in a cross section where the hard interaction process is described by a hard function while all the low energy QCD effects are contained in beam and soft functions. The factorization enables one to perform the necessary resummation in the low $\mathbf{p}_\perp^2$ region separately for each sector. An important observable of interest that can be computed within this framework is the $\mathbf{p}_\perp^2$ spectrum of Higgs production at the LHC.

The soft function can be calculated perturbatively; however it suffers from rapidity divergences. These arise from the factorization and are connected to large rapidity logarithms that need to be resummed. We have calculated the soft function up to NNLO in a previously invented framework [8] that introduces a rapidity regulator in addition to dimensional regularization. This rapidity regulator comes with an additional renormalization scale that yields a RRGE and solving this RRGE amounts to resumming all the rapidity logarithms. We went through the renormalization procedure of the soft function and the computation of all anomalous dimensions in detail. The results have been presented in both momentum and position space.

In our computation of the soft function we assumed the rapidity regulator to preserve exponentiation and used the non-abelian exponentiation theorem to retrieve the C_F^2 piece. This has however not been checked explicitly and it would be interesting to go through the calculation of the C_F^2 diagrams as well, which is left to future work.

We have also seen how the renormalization group structure of the theory can be a powerful tool when it comes to predicting the form of the perturbation series. From the known structure of the μ anomalous dimension, we derived a recursive relation for the structure of the beam and soft functions to all orders. Agreement between this structure and our results provides a strong cross check of our calculations.

Knowing the structure of our beam and soft functions, we were able to derive the full results for the beam functions in our framework as well, without explicitly calculating them. This was done by comparing our results to results within another framework. We have shown that the two frameworks yield the same result after performing the resummation of rapidity logarithms. However, the formalism used in this thesis enables one to directly probe uncertainties associated with variations of rapidity scales.

In conclusion, we have calculated the transverse momentum dependent soft function in SCET to NNLO for $pp \to XL$, in the region $\mathbf{p}_\perp^2 \ll Q^2$. By knowing the renormalization group structure of the theory, we extracted the beam functions to NNLO from known results. With these ingredients, one can now compute the mentioned cross section to NNLL$'$ for the first time in this formalism. In addition, this enables one to perform the complete set of relevant scale variations in order to estimate the uncertainty in the resummed cross section.

Acknowledgments

This project was conducted at DESY-Hamburg and first of all I would like to thank Frank Tackmann for the invitation. DESY is a great research institute and working there has been a very educating experience.

This thesis could not have been done if it was not for all the help, guidance, wisdom and support from my fellow physicist friends in the penthouse suite of 1b. There is a lot of joy and misery in learning that we, more often than not, have to fail before we succeed in our calculations. A special thanks to Markus Ebert, Thomas Luebbert, Maximilian Stahlhofen and Frank Tackmann for all the physics discussions and support in this project.

All diagrams and pictures were created with Jaxodraw [35].

Appendix A

Renormalization Conventions

Throughout this thesis we use the $\overline{\text{MS}}$ scheme which amounts to renormalizing the coupling constant in the following way,

$$\alpha_s^b \to \mu^{2\epsilon}\alpha_s(\mu)\frac{e^{\epsilon\gamma_E}}{(4\pi)^\epsilon}\left(1-\beta_0\frac{\alpha_s}{4\pi}\frac{1}{\epsilon}+\mathcal{O}(\alpha_s^2)\right). \tag{A.1}$$

This has a consequence when computing the derivative of $\alpha_s(\mu)$ since there is a ϵ term as well as the beta function,

$$\mu\frac{d}{d\mu}\alpha_s(\mu) = -2\epsilon\alpha_s(\mu)+\beta[\alpha_s(\mu)]. \tag{A.2}$$

The beta function is

$$\beta[\alpha_s] = -2\alpha_s\sum_{n=0}^{\infty}\beta_n\left(\frac{\alpha_s}{4\pi}\right)^{n+1}, \tag{A.3}$$

$$\beta_0 = \frac{11C_A-4T_Fn_f}{3}, \tag{A.4}$$

$$\beta_1 = \frac{34}{3}C_A^2-\left(\frac{20}{3}C_A+4C_F\right)T_Fn_f. \tag{A.5}$$

In the case of QCD, the group factors are $T_F=\frac{1}{2}$, $C_A=N_c=3$ and $C_F=\frac{4}{3}$.

We also renormalize the book keeping parameter w, so it obeys

$$\nu\frac{d}{d\nu}w = -\frac{\eta}{2}w. \tag{A.6}$$

Parts of the anomalous dimensions can be written in terms of the cusp anomalous dimension which is known up to three loops. Here we denote it as

$$\Gamma^i_{\text{cusp}} = \sum_{n=0}^{\infty}\Gamma^i_n\left(\frac{\alpha_s}{4\pi}\right)^{n+1}, \tag{A.7}$$

where the quark coefficients are

$$\begin{aligned}\Gamma^q_0 =& 4C_F,\\ \Gamma^q_1 =& 4C_F\left[\left(\frac{67}{9}-\frac{\pi^2}{3}\right)C_A-\frac{20}{9}T_Fn_f\right],\end{aligned} \tag{A.8}$$

and are equal to $\frac{C_F}{C_A}\Gamma^g_{0,1}$.

Appendix B

Feynman rules for Wilson lines

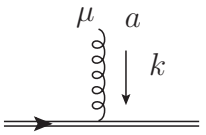

$$= \frac{-gn^\mu t^a}{n\cdot k}$$

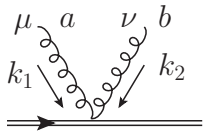

$$= n^\mu n^\nu \left[\frac{t^a t^b}{n\cdot k_1 n\cdot(k_1+k_2)} + \frac{t^b t^a}{n\cdot k_2 n\cdot(k_1+k_2)}\right]$$

Figure B.1: Feynman rules for a S_n Wilson line.

The Wilson lines are path ordered exponential of gauge fields. In the soft function we will come across the Wilson lines for an incoming quark/antiquark(quark along the n direction)

$$\begin{aligned} S_n(x) =& \mathbf{P}\exp\left[ig\int_{-\infty}^{0} ds n\cdot A(x+sn)\right], \\ S_{\bar{n}}^\dagger(x) =& \bar{\mathbf{P}}\exp\left[-ig\int_{-\infty}^{0} ds \bar{n}\cdot A(x+s\bar{n})\right]. \end{aligned}$$

If we first look at a single emission in the S_n, we can expand and Fourier transform to get the Feynman rules in momentum space[1]. This evaluates to

$$\begin{aligned} S_n(x) = \mathbf{P}\exp\left[ig\int_{-\infty}^{0} ds n\cdot A(x+sn)\right] &= 1 + ig\int_{-\infty}^{0} ds n\cdot A(x+xn) + \mathcal{O}(g^2) \\ &= 1 + ig\int_{-\infty}^{0} ds \int \frac{d^4k}{(2\pi)^4} e^{-ik\cdot(x+sn)} n^\mu A_\mu^a(k) t^a + \mathcal{O}(g^2) \\ &= 1 + \int \frac{d^dk}{(2\pi)^d}\left(\frac{-gn^\mu t^a}{n\cdot k + i\varepsilon}\right)\tilde{A}_\mu^a e^{-ik\cdot x} + \mathcal{O}(g^2). \end{aligned} \quad \text{(B.1)}$$

This is the well known eikonal vertex approximation and this results can also be obtained from the soft gluon limit of the single gluon emission diagram in QCD.

[1] To make the fourier transform finite, we send $k \to k + i\varepsilon$.

Similarly the next order term in the expansion of S_n is

$$\frac{g^2}{2}\int\frac{d^4k_1}{(2\pi)^4}\int\frac{d^4k_2}{(2\pi)^4}n^\mu n^\nu\left[\frac{t^at^b}{(n\cdot k_1+i\varepsilon)[n\cdot(k_1+k_2)+i\varepsilon]}+\frac{t^bt^a}{(n\cdot k_2+i\varepsilon)[n\cdot(k_1+k_2)+i\varepsilon]}\right]\times\tilde{A}^a_\mu\tilde{A}^b_\nu e^{-i(k_1+k_2)\cdot x}. \quad \text{(B.2)}$$

From these equations one can read off the Feynman rules in momentum space, see Fig. B.1. The full momentum version of the Wilson line we write as[2]

$$S_n=\sum_{n=0}^{\infty}\sum_{\text{perms}}\frac{(-g)^n}{n!}\frac{n\cdot A(k_1)\cdots n\cdot A(k_n)}{[n\cdot k_1][n\cdot(k_1+k_2)]\cdots[n\cdot(\sum_{i=1}^n k_i)]}. \quad \text{(B.3)}$$

Different Wilson lines gives different signs for the $i\varepsilon$ terms and the different combinations can be seen in Fig. B.2.

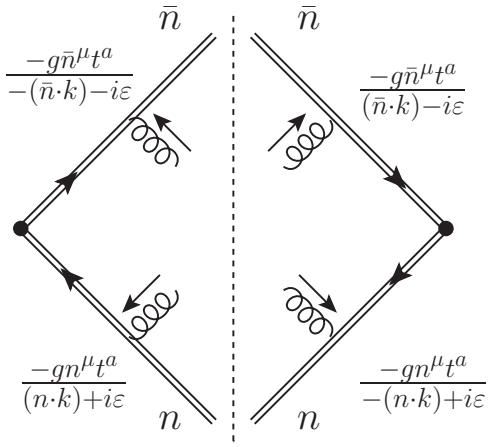

Figure B.2: Feynman rules for a soft function in the fundamental representation.

[2]Here we suppress all $+i\varepsilon$ terms in the propagators.

Appendix C

Plus Distributions

In our calculations we will often find integrals over two functions, $f(x)$ and $g(x)$ where $f(x)$ has a pole at $a \in [b, c]$ while $g(x)$ is finite at that point. If we add $g(a) - g(a) = 0$ we can write the integral as

$$\int_b^c dx f(x)g(x) = g(a)\int_b^c dx f(x) + \int_b^c dx f(x)[g(x) - g(a)]. \tag{C.1}$$

The second term is then fine and we can define it as an integration of a plus distribution which we can write as

$$[f(x)]_+^{[b,c]} \equiv -\delta(x-a)\int_b^c dx' f(x') + f(x) \tag{C.2}$$

For the case $f(x) = x^{-1+\alpha}$ on $[0, 1]$ we can derive a useful identity by writing

$$\frac{1}{x^{1-\alpha}} = \frac{\delta(x)}{\alpha} + \left[\frac{1}{x^{1-\alpha}}\right]_+ = \frac{\delta(x)}{\alpha} + \sum_{n=0}^{\infty}\frac{\alpha^n}{n!}\left[\frac{1}{x}\log^n x\right]_+. \tag{C.3}$$

2-dimensional plus distributions

Plus distributions will be encountered in the 2-dimensional $p_\perp$ space in this thesis and they can then conveniently be defined with dimensional regularization as

$$\int \frac{d^2\mathbf{p}}{(2\pi)^2} f(\mathbf{p})\left[P(\mathbf{p},\mu)\right]_+ \equiv \lim_{\epsilon\to 0^+}\mu^{-2\epsilon}\left\{\int \frac{d^{2+2\epsilon}\mathbf{p}}{(2\pi)^{2+2\epsilon}} f(\mathbf{p})P(\mathbf{p},\mu) - f(0)\int_{\mathcal{D}\mu}\frac{d^{2+2\epsilon}\mathbf{p}}{(2\pi)^{2+2\epsilon}}P(\mathbf{p},\mu)\right\}, \tag{C.4}$$

where $\mathcal{D}\mu = \{\mathbf{p} : |\mathbf{p}| < \mu\}$. Throughout this thesis we encounter a certain class of plus distributions which we define to be

$$\mathcal{L}_n(\mathbf{p}^2,\mu^2) = \frac{1}{2\pi\mu^2}\left[\frac{\mu^2}{\mathbf{p}^2}\log^n\left(\frac{\mu^2}{\mathbf{p}^2}\right)\right]_+ \tag{C.5}$$

and the useful identity then becomes

$$\frac{1}{\mu^2}\left(\frac{\mu^2}{\mathbf{p}^2}\right)^{1+\alpha} = -\frac{\pi\delta^{(2)}(\mathbf{p})}{\alpha} + 2\pi\mathcal{L}^\alpha = -\frac{\pi\delta^{(2)}(\mathbf{p})}{\alpha} + 2\pi\sum_{n=0}^{\infty}\frac{\alpha^n}{n!}\mathcal{L}_n. \tag{C.6}$$

where we have defined the plus distribution

$$\mathcal{L}^\alpha = \frac{1}{2\pi\mu^2}\left[\left(\frac{\mu^2}{\mathbf{p}^2}\right)^{1+\alpha}\right]_+ = \sum_{n=0}^{\infty}\frac{\alpha^n}{n!}\mathcal{L}_n. \tag{C.7}$$

The derivative of $\mathcal{L}_n$ can be shown to obey

$$\mu\frac{d}{d\mu}\mathcal{L}_0 = -\delta^{(2)}(\mathbf{p}), \tag{C.8}$$

$$\mu\frac{d}{d\mu}\mathcal{L}_n = 2n\mathcal{L}_{n-1}. \tag{C.9}$$

Convolutions

In the renormalization process one also need the convolutions of plus distributions. We can get them from the equation [8]

$$\mathcal{L}^\alpha \otimes_\perp \mathcal{L}^\beta(\mathbf{p}) = \frac{U(\alpha,\beta)}{2\pi}\mathcal{L}^{\alpha+\beta} + \frac{1}{8\pi^2\alpha}\mathcal{L}^\beta + \frac{1}{8\pi^2\beta}\mathcal{L}^\alpha - \delta^{(2)}(\mathbf{p})\left[\frac{U(\alpha,\beta)}{4\pi(\alpha+\beta)} + \frac{1}{16\pi^2\alpha\beta}\right], \tag{C.10}$$

where

$$U(\alpha,\beta) = \frac{\Gamma(1+\alpha+\beta)}{4\pi\Gamma(1+\alpha)\Gamma(1+\beta)}\frac{\Gamma(-\alpha)\Gamma(-\beta)}{\Gamma(-\alpha-\beta)}. \tag{C.11}$$

By expanding the plus distributions in Eq. (C.10) and matching up the coefficients one then arrives at the convolutions for the $\mathcal{L}_n$'s. The lowest order ones are

$$\mathcal{L}_0 \otimes_\perp \mathcal{L}_0 = -\frac{1}{4\pi^2}\mathcal{L}_1, \tag{C.12}$$

$$\mathcal{L}_0 \otimes_\perp \mathcal{L}_1 = -\frac{3}{16\pi^2}\mathcal{L}_2 + \delta^{(2)}(\mathbf{p})\frac{\psi^{(2)}(1)}{16\pi^2}, \tag{C.13}$$

$$\mathcal{L}_0 \otimes_\perp \mathcal{L}_2 = -\frac{1}{6\pi^2}\mathcal{L}_3 - \frac{\psi^{(2)}(1)}{4\pi^2}\mathcal{L}_0, \tag{C.14}$$

$$\mathcal{L}_1 \otimes_\perp \mathcal{L}_1 = -\frac{1}{8\pi^2}\mathcal{L}_3 - \frac{\psi^{(2)}(1)}{4\pi^2}\mathcal{L}_0, \tag{C.15}$$

$$\mathcal{L}_1 \otimes_\perp \mathcal{L}_2 = -\frac{5}{48\pi^2}\mathcal{L}_4 + \frac{3\zeta(3)}{2\pi^2}\mathcal{L}_1 + \delta^{(2)}(\mathbf{p})\frac{\psi^{(4)}(1)}{48\pi^2}. \tag{C.16}$$

Fourier Transform

Some of the calculations and results are simpler in position space where there are no convolutions. The fourier transform of the plus distributions can be retrieved from the equation

$$\int\frac{d^2\mathbf{p}}{(2\pi)^2}e^{i\mathbf{b}\cdot\mathbf{p}}\frac{1}{\mu^2}\left(\frac{\mu^2}{\mathbf{p}^2}\right)^{1+\alpha} = -\frac{e^{-2\alpha\gamma_E}}{4\pi\alpha}\frac{\Gamma(1-\alpha)}{\Gamma(1+\alpha)}\left(\frac{\mathbf{b}^2\mu^2e^{2\gamma_E}}{4}\right)^\alpha \tag{C.17}$$

by using Eq. (C.6) and expanding in powers of α. Some of the lowest ones are shown in Tab. C.1 and C.2.

p-space	**b**-space
$\delta^{(2)}(\mathbf{p})$	$\frac{1}{(2\pi)^2}$
$\mathcal{L}_0$	$-\frac{1}{8\pi^2}L_b$
$\mathcal{L}_1$	$-\frac{1}{16\pi^2}L_b^2$
$\mathcal{L}_2$	$-\frac{1}{24\pi^2}\left[L_b^3+4\zeta(3)\right]$
$\mathcal{L}_3$	$-\frac{1}{32\pi^2}\left[L_b^4+16\zeta(3)L_b\right]$
$\mathcal{L}_4$	$-\frac{1}{40\pi^2}\left[L_b^5+40\zeta(3)L_b+48\zeta(5)\right]$

Table C.1: Fourier transforms of plus distributions in terms of $L_b = \log\left(\frac{\mathbf{b}^2\mu^2 e^{2\gamma_E}}{4}\right)$.

p-space	**b**-space
1	$(2\pi)^2\delta^{(2)}(\mathbf{p}) = \mathbb{I}_p$
L_b	$-8\pi^2\mathcal{L}_0$
L_b^2	$-16\pi^2\mathcal{L}_1$
L_b^3	$-24\pi^2\mathcal{L}_2 - 4\zeta(3)\mathbb{I}_p$
L_b^4	$-32\pi^2\left[\mathcal{L}_3 - 4\zeta(3)\mathcal{L}_0\right]$

Table C.2: Fourier transforms of $L_b = \log\left(\frac{\mathbf{b}^2\mu^2 e^{2\gamma_E}}{4}\right)$ to momentum space in terms of plus distributions.

Appendix D

Hypergeometric Functions

When solving some of the 2-loop integrals we come across Hypergeometric functions. We present some relevant facts about them below but refer to Ref. [36, 37] for further details.

Their general form ${}_pF_q(a_1,\ldots,a_p;b_1,\ldots,b_q;z)$ is defined as the solution $f(z)$ to the differential equation

$$z\prod_{n=1}^{p}\left(z\frac{d}{dz}+a_n\right)f(z)=z\frac{d}{dz}\prod_{m=1}^{q}\left(z\frac{d}{dz}+b_m-1\right)f(z). \tag{D.1}$$

It can be written down as a power series with the help of the Pochhammer symbol

$$(a_i)_n=\frac{\Gamma(a_i+n)}{\Gamma(a_i)}, \tag{D.2}$$

as

$${}_pF_q(a_1,\ldots,a_p;b_1,\ldots,b_q;z)={}_pF_q\left(\begin{matrix}a_1,\ldots,a_p\\ b_1,\ldots,b_q\end{matrix};z\right)=\sum_{n=0}^{\infty}\frac{(a_1)_n\cdots(a_p)_n}{(b_1)_n\cdots(b_q)_n}\frac{z^n}{n!} \tag{D.3}$$

as long as all $b_i\notin-\mathbb{N}_0$. It is from this notation clear that we can freely change the ordering in the $\{a_i\}$ and $\{b_i\}$ sets. Moreover, if we have any $a_i=b_j$ they cancel which reduces ${}_pF_q$ to ${}_{p-1}F_{q-1}$.

The analytic properties of ${}_pF_q$ is as follows: Any a_i can be a non-positive integer and in that case only the first $-a_i$ terms in Eq. (D.3) are non-zero. The Hypergeometric function then has an infinite radius of convergence.

For $p\leq q$, the series converges for all finite values of z and if $p>q+1$ the series generally diverges for non-zero z.

In this thesis we will only deal with functions where $p=q+1$ where the radius of convergence is 1. We define the number

$$\gamma=(b_1+\ldots+b_q)-(a_1+\ldots+a_p). \tag{D.4}$$

The function is then absolutely convergent for $|z|=1$ if the real part of γ is positive, $\Re(\gamma)>0$, convergent except at $z=1$ for $-1<\Re(\gamma)\leq 0$ and divergent for $\Re(\gamma)\leq -1$.

In some cases one might have to extract the divergent part of a ${}_2F_1$. This can be done with an Euler transformation

$${}_2F_1(a,b;c,z)=(1-x)^{c-a-b}{}_2F_1(c-a,c-b;c,z), \tag{D.5}$$

which makes $\Re(\gamma)>0$ positive.

Integral Representation

Instead of defining the Hypergeometric series as a power series one can define them in a recursive integral representation where

$$ {}_{p+1}F_{q+1}\left(\begin{matrix} a_0, a_1, \ldots, a_p \\ b_0, b_1, \ldots, b_q \end{matrix}; z\right) = \frac{\Gamma(b_0)}{\Gamma(a_0)\Gamma(b_0 - a_0)} \times \int_0^1 dy y^{a_0-1}(1-y)^{b_0-a_0-1} {}_pF_q\left(\begin{matrix} a_1, \ldots, a_p \\ b_1, \ldots, b_q \end{matrix}; zy\right), \quad \text{(D.6)} $$

assuming $\mathbb{R}(b_0) > \mathbb{R}(a_0) > 0$. For $p = q + 1$ this holds if $|\arg(1 - z)| < \pi$. The Hypergeometric functions with a low number of arguments are familiar functions such as

$$ {}_1F_0(a;;z) = (1-z)^{-a}, \quad \text{(D.7)} $$

$$ {}_0F_0(;;z) = e^z. \quad \text{(D.8)} $$

This integral representation will prove useful since it shows up directly in the 2-loop calculation.

D.1 Expansion

When computing the soft function, we can always express the final result in a closed form in terms of Hypergeometric functions as in Eq. (5.41)-(5.44). However that is not so useful and we eventually want to expand the result in η and ϵ. If the Hypergeometric contains a non-positive a_i then it is a simple task because it can be written down as a series of gamma functions with $-a_i$ terms. Thus one can see that the $\mathcal{G}$, $\mathcal{H}$ and $\mathcal{Q}$ contributions, although they appear rather lengthy, are really the simplest.

In the other cases we need to expand ${}_3F_2$ functions. We made use of the mathematica package HypExp [28] to arrive at the following expansions:

$$ \begin{aligned} I(1,1,0,0-\epsilon-\frac{\eta}{2},\epsilon) =& \frac{1}{\epsilon^2} + \frac{\pi^2}{3} + 4\zeta(3)\epsilon + \frac{11\pi^4}{90}\epsilon^2 \\ &+ \left[\frac{\pi^2}{6\epsilon} + \frac{17\pi^4}{360}\epsilon + \left(8\zeta(5) - \frac{\pi^2}{2}\zeta(3)\right)\epsilon^2\right]\eta \\ &+ \mathcal{O}(\epsilon^3) + \mathcal{O}(\eta^2), \end{aligned} \quad \text{(D.9)} $$

$$ \begin{aligned} I(0,1,1,0,-\epsilon-\frac{\eta}{2},\epsilon) =& -\frac{\pi^2}{3} + 2\zeta(3)\epsilon - \frac{\pi^4}{45}\epsilon^2 + \left[\frac{2\pi^2}{3}\zeta(3) + 2\zeta(5)\right]\epsilon^3 \\ &+ \left[-\frac{4}{\epsilon} + 8\zeta(3)\epsilon^2 + \frac{2\pi^4}{15}\epsilon^3\right]\frac{1}{\eta} \\ &+ \left[\zeta(3) - \frac{11\pi^4}{360}\epsilon + \left(\frac{\pi^2}{6}\zeta(3) + 2\zeta(5)\right)\epsilon^2 + \left(-\frac{17\pi^6}{3780} - \frac{5\zeta(3)^2}{2}\right)\epsilon^3\right]\eta \\ &+ \mathcal{O}(\epsilon^4) + \mathcal{O}(\eta^2). \end{aligned} \quad \text{(D.10)} $$

From the $\mathcal{T}$ diagram we get a $I(0,1,1,-\epsilon-\frac{\eta}{2},1+\epsilon)$ term which contains a ${}_3F_2$ that could not be expanded with HypExp. However one can go back to the integral representation with Eq. (D.6) and expand the ${}_2F_1$ function and then integrate all the terms separately.

Doing this gives

$$\begin{aligned} I(0,1,1,-\epsilon-\frac{\eta}{2},1+\epsilon) =& \frac{2}{\epsilon^2}-\frac{2\pi^2}{3}-4\zeta(3)\epsilon-\frac{\pi^4}{9}\epsilon^2+\left[\frac{4\pi^2}{3}\zeta(3)-12\zeta(5)\right]\epsilon^3 \\ &+\left[-\frac{4}{\epsilon}+8\zeta(3)\epsilon^2+\frac{19\pi^4}{90}\epsilon^3\right]\frac{1}{\eta} \\ &+\left[\frac{\pi^2}{6\epsilon}+2\zeta(3)-\frac{17\pi^4}{360}\epsilon-\frac{2\pi^2}{3}\zeta(3)\epsilon^2\right]\eta \\ &+\mathcal{O}(\epsilon^4)+\mathcal{O}(\epsilon^3\eta)+\mathcal{O}(\eta^2). \end{aligned} \tag{D.11}$$

Appendix E

Wilson Coefficients for Higgs Production

The $\mathbf{p}_\perp^2$ differential cross section for Higgs production can be found in Eq. (7.11), where the Born cross section is

$$\sigma_0(\mu) = \frac{m_h^2 \alpha_s^2(\mu)}{72\pi(N_c^2-1)sv^2}, \tag{E.1}$$

and the Wilson coefficients are [38]

$$C_t^2(m_t^2,\mu)|C_S(-m_h^2,\mu)|^2 = 1 + c_1\left(\frac{\alpha_s}{4\pi}\right) + c_2\left(\frac{\alpha_s}{4\pi}\right)^2 + \dots, \tag{E.2}$$

$$\tag{E.3}$$

where

$$\begin{aligned} c_1 =& -6\log^2\frac{m_h^2}{\mu^2} + 22 + 7\pi^2, \\ c_2 =& 18\log^4\frac{m_h^2}{\mu^2} + \frac{46}{3}\log^3\frac{m_h^2}{\mu^2} + \left(-\frac{698}{3} - 36\pi^2\right)\log^2\frac{m_h^2}{\mu^2} \\ & - \frac{274}{3}\log\frac{m_t^2}{\mu^2} + \left(\frac{1240}{9} - \frac{184\pi^2}{3} - 36\zeta(3)\right)\log\frac{m_h^2}{\mu^2} \\ & + \frac{10718}{27} + \frac{1679\pi^2}{6} - \frac{998\zeta(3)}{3} + \frac{37\pi^4}{2}. \end{aligned}$$

Bibliography

[1] **ATLAS** Collaboration, G. Aad et al., *Observation of a new particle in the search for the Standard Model Higgs boson with the ATLAS detector at the LHC*, *Phys.Lett.* **B716** (2012) 1–29, [arXiv:1207.7214].

[2] **CMS** Collaboration, S. Chatrchyan et al., *Observation of a new boson at a mass of 125 GeV with the CMS experiment at the LHC*, *Phys.Lett.* **B716** (2012) 30–61, [arXiv:1207.7235].

[3] P. W. Higgs, *Broken Symmetries and the Masses of Gauge Bosons*, *Phys.Rev.Lett.* **13** (1964) 508–509.

[4] F. Englert and R. Brout, *Broken Symmetry and the Mass of Gauge Vector Mesons*, *Phys.Rev.Lett.* **13** (1964) 321–323.

[5] **ATLAS** Collaboration, G. Aad et al., *Measurements of the Total and Differential Higgs Boson Production Cross Sections Combining the $H \to \gamma\gamma$ and $H \to ZZ^* \to 4\ell$ Decay Channels at $\sqrt{s} = 8$ TeV with the ATLAS Detector*, arXiv:1504.05833.

[6] J. C. Collins, D. E. Soper, and G. F. Sterman, *Transverse Momentum Distribution in Drell-Yan Pair and W and Z Boson Production*, *Nucl.Phys.* **B250** (1985) 199.

[7] D. de Florian and M. Grazzini, *The Structure of large logarithmic corrections at small transverse momentum in hadronic collisions*, *Nucl. Phys.* **B616** (2001) 247–285, [hep-ph/0108273].

[8] J.-Y. Chiu, A. Jain, D. Neill, and I. Z. Rothstein, *A Formalism for the Systematic Treatment of Rapidity Logarithms in Quantum Field Theory*, *JHEP* **1205** (2012) 084, [arXiv:1202.0814].

[9] J.-y. Chiu, A. Jain, D. Neill, and I. Z. Rothstein, *The Rapidity Renormalization Group*, *Phys.Rev.Lett.* **108** (2012) 151601, [arXiv:1104.0881].

[10] T. Becher, M. Neubert, and D. Wilhelm, *Higgs-Boson Production at Small Transverse Momentum*, *JHEP* **1305** (2013) 110, [arXiv:1212.2621].

[11] D. Neill, I. Z. Rothstein, and V. Vaidya, *The Higgs Transverse Momentum Distribution at NNLL and its Theoretical Errors*, arXiv:1503.00005.

[12] T. Gehrmann, T. Luebbert, and L. L. Yang, *Calculation of the transverse parton distribution functions at next-to-next-to-leading order*, *JHEP* **1406** (2014) 155, [arXiv:1403.6451].

[13] T. Gehrmann, T. Lubbert, and L. L. Yang, *Transverse parton distribution functions at next-to-next-to-leading order: the quark-to-quark case*, *Phys. Rev. Lett.* **109** (2012) 242003, [arXiv:1209.0682].

[14] C. W. Bauer, S. Fleming, and M. E. Luke, *Summing Sudakov logarithms in B —> X(s gamma) in effective field theory*, *Phys.Rev.* **D63** (2000) 014006, [hep-ph/0005275].

[15] C. W. Bauer, S. Fleming, D. Pirjol, and I. W. Stewart, *An Effective field theory for collinear and soft gluons: Heavy to light decays*, *Phys.Rev.* **D63** (2001) 114020, [hep-ph/0011336].

[16] C. W. Bauer and I. W. Stewart, *Invariant operators in collinear effective theory*, *Phys.Lett.* **B516** (2001) 134–142, [hep-ph/0107001].

[17] C. W. Bauer, D. Pirjol, and I. W. Stewart, *Soft collinear factorization in effective field theory*, *Phys.Rev.* **D65** (2002) 054022, [hep-ph/0109045].

[18] I. W. Stewart, F. J. Tackmann, and W. J. Waalewijn, *Factorization at the LHC: From PDFs to Initial State Jets*, *Phys.Rev.* **D81** (2010) 094035, [arXiv:0910.0467].

[19] J. C. Collins, D. E. Soper, and G. F. Sterman, *Soft Gluons and Factorization*, *Nucl. Phys.* **B308** (1988) 833.

[20] T. Becher, A. Broggio, and A. Ferroglia, *Introduction to Soft-Collinear Effective Theory*, arXiv:1410.1892.

[21] I. W. Stewart, "Lectures on the soft-collinear effective theory." 2013.

[22] C. W. Bauer, D. Pirjol, and I. W. Stewart, *Factorization and endpoint singularities in heavy to light decays*, *Phys. Rev.* **D67** (2003) 071502, [hep-ph/0211069].

[23] J. Frenkel and J. Taylor, *NONABELIAN EIKONAL EXPONENTIATION*, *Nucl.Phys.* **B246** (1984) 231.

[24] J. Gatheral, *Exponentiation of Eikonal Cross-sections in Nonabelian Gauge Theories*, *Phys.Lett.* **B133** (1983) 90.

[25] P. F. Monni, T. Gehrmann, and G. Luisoni, *Two-Loop Soft Corrections and Resummation of the Thrust Distribution in the Dijet Region*, *JHEP* **1108** (2011) 010, [arXiv:1105.4560].

[26] T. Lubbert, *Transverse parton distribution functions at next-to-next-to-leading order*. PhD thesis, University of Zurich, http://opac.nebis.ch/ediss/20142048.pdf, 2014.

[27] A. Hornig, C. Lee, I. W. Stewart, J. R. Walsh, and S. Zuberi, *Non-global Structure of the $O(\alpha_s^2)$ Dijet Soft Function*, *JHEP* **1108** (2011) 054, [arXiv:1105.4628].

[28] T. Huber and D. Maitre, *HypExp 2, Expanding Hypergeometric Functions about Half-Integer Parameters*, *Comput.Phys.Commun.* **178** (2008) 755–776, [arXiv:0708.2443].

[29] J. R. Gaunt, M. Stahlhofen, and F. J. Tackmann, *The Quark Beam Function at Two Loops*, *JHEP* **04** (2014) 113, [arXiv:1401.5478].

[30] J. Gaunt, M. Stahlhofen, and F. J. Tackmann, *The Gluon Beam Function at Two Loops*, *JHEP* **1408** (2014) 020, [arXiv:1405.1044].

[31] T. Becher, M. Neubert, and D. Wilhelm, *Electroweak Gauge-Boson Production at Small q_T: Infrared Safety from the Collinear Anomaly*, *JHEP* **02** (2012) 124, [arXiv:1109.6027].

[32] T. Becher and M. Neubert, *Drell-Yan Production at Small q_T, Transverse Parton Distributions and the Collinear Anomaly*, *Eur. Phys. J.* **C71** (2011) 1665, [arXiv:1007.4005].

[33] L. G. Almeida, S. D. Ellis, C. Lee, G. Sterman, I. Sung, and J. R. Walsh, *Comparing and counting logs in direct and effective methods of QCD resummation*, *JHEP* **04** (2014) 174, [arXiv:1401.4460].

[34] I. W. Stewart, F. J. Tackmann, and W. J. Waalewijn, *The Quark Beam Function at NNLL*, *JHEP* **09** (2010) 005, [arXiv:1002.2213].

[35] D. Binosi and L. Theussl, *JaxoDraw: A Graphical user interface for drawing Feynman diagrams*, *Comput.Phys.Commun.* **161** (2004) 76–86, [hep-ph/0309015].

[36] R. F.Olver, D.Lozier and C.Clark, *NIST Handbook of Mathematical Functions*. Cambridge University Press, 2010.

[37] Bateman, *Higher Transcendental Functions*. McGraw-Hill Book Co, 1955.

[38] T. Becher and M. Neubert, *Factorization and NNLL Resummation for Higgs Production with a Jet Veto*, *JHEP* **07** (2012) 108, [arXiv:1205.3806].